Sánchez-Delgado, S., Marugán-Cruz, C., Serrano, D. & Briongos, J. (2019). Distributor performance in a bubbling fluidized bed: Effects of multiple gas inlet jet and bubble generation. *Chemical Engineering Science*, vol. 195, pp. 367–380.

DOI: 10.1016/j.ces.2018.09.035

Distributor performance in a bubbling fluidized bed: effects of multiple gas inlet jet and bubble generation.

Sánchez-Delgado S.*, Marugán-Cruz C., Serrano D. and Briongos J.V.

Energy Systems Engineering Research Group, Thermal and Fluid Engineering Department, Carlos III University of Madrid, Leganés (Madrid), Spain

* Corresponding autor: e-mail address: sergio.sanchez@uc3m.es (Sánchez-Delgado S.)

Abstract

This work presents a study of the effect of the distributor performance in the bubble generation, growth and interaction within a bubbling fluidized bed. In order to characterize this effect in short-term and long-term dynamics, as well as in time and frequency domain, classical and innovative techniques (Digital Image Analysis, DIA, and Wavelet Analysis WA, respectively) have been used over the images acquired in a two dimensional bubbling fluidized bed.

Four perforated plate distributors, with the same open area and the same pressure drop, have been used in the experiments, varying the excess gas and the fixed bed height to study the effect of this operation conditions. The results reveal that the distributor performance has no effect in the mean bubble behavior of the bubbles within the fluidized bed, and therefore there is no effect in the long-term dynamics of the fluidized bed. The analysis, performed on the bubble generation region, also reveals that the distributor as no effect on the bubble generation frequency. However, it can be concluded that distributor performance has a great influence in the bubble generation location along the distributor, being the most homogenously distributed generation profiles, those in which the distributor with the largest numbers of holes and smaller diameter has been used. The distributor affects importantly the total number of bubbles (the higher the number of holes the more bubbles are generated). The fixed bed height does not affect the PDF (Probability Density Function) of the bubbles along the distributor, however the PDF of the bubbles along the distributor presents more homogenous profiles at higher values of the excess gas. These results reveal the great importance of the distributor type in the modelling of bubbling phenomena, but only in the bubble generation region, since from this region the fluidized bed dynamics is not affected for the distributor type.

Keywords:

Distributor performance, Fluidized beds, bubble generation, Wavelet Coherent Analysis, time dependent dynamics, multiple gas jet.

Abbreviations:

AAFT: Amplitude Adjusted Fourier Transform

BVF: Bubble Void Fraction

COI: Cone Of Influence

DIA: Digital Image Analysis

JR: Jet Region

PDF: Probability Density Function

PSD: Power Spectral Density

ROI: Region of Interest

WCA: Wavelet Coherence Analysis

1. Introduction

Fluidized bed systems are frequently used for many industrial applications, due to their high mixing and heating rates: solids drying and mixing, thermochemical conversion or cracking processes (Adánez et al., 2018; Haron et al., 2017; G. Li et al., 2018). However, the complexities of the dynamics characterizing gas-solid fluidized beds lead to design uncertainties that endanger the satisfactory operational characteristics of the industrial units. Factors such as undesirable gas flow or solid flow circulation patterns can lead to operational problems such as unscheduled shutdowns or poor operation performance.

The distributor design is broadly accepted by the fluidization community to directly influence the generation, growing and interaction of bubbles, acting on the fluidization quality, which defines the gas solid fluidized behavior in terms of solid mixing and heat transfer. Accordingly, idea large collection of work can be found in the scientific literature regarding the distributor design (Briens et al., 1997; Eow et al., 2003; Geldart and Baeyens, 1985; Lombardi et al., 1997; Qureshi and Creasy, 1979; Sánchez-Prieto et al., 2014; Sathiy Amoorthy and Sridhar Rao, 1979; Sathiyamoorthy and Horio, 2003; Sathiyamoorthy and Sridhar Rao, 1981, 1978; Saxena et al., 1979; Thorpe et al., 2002; Walker, 1975). For most applications, the distribution design aims to obtain a homogeneous distribution of air in the whole section of the reactor, avoiding dead zones (nonfluidized regions), bubble channeling zones or minimizing the attrition of the bed material. Until now, there are many experimental research articles, that study the bubble phase and the dense phase, in order to determine the dynamics of the fluid

bed (Gómez-Hernández et al., 2017; Helmi et al., 2018; Sánchez-Delgado et al., 2010a), the sizes and velocities of the bubbles (Lau et al., 2013; Laverman et al., 2008; Maurer et al., 2016; Sánchez-Delgado et al., 2013a; Shen et al., 2004; Sobrino et al., 2009b, 2009a), as well as the velocity of the particles of the dense phase and the solid mixing within the fluidized bed (Bakshi et al., 2017; Y. Li et al., 2018; Sánchez-Delgado et al., 2013a, 2010a).

However, to the authors' knowledge, none of these studies tries to explore the relation between the distributor design and the long-term bed dynamics. Nonlinear science makes possible to make use of advance data treatments that account for the multi scale nature of gas-solid fluidized bed systems (Marwan et al., 2007; Villa Briongos et al., 2006). In this line, wavelet analysis has become the most popular tool for multiscale analysis of complex dynamics (Donoho and Johnstone, 1995; Grinsted et al., 2004; He et al., 2009; Labat, 2005; Lu and Li, 1999). New measures such as the wavelet entropy (Zunino et al., 2007) or the wavelet coherence (Clemson et al., 2016; Grinsted et al., 2004) have shown that the wavelet analysis produces more information than just qualitative results. Moreover, the complexity characterizing gas-solid fluidized bed dynamics give rise to a huge amount of theoretical research effort addressed to understand the different dynamical structures such as bubbles or particle clusters appearing in fluidized beds (Chen et al., 2017). On the one hand, either continuum, Eulerian-Eulerian, Eulerian-Lagrange or discrete approach models, are currently used to study fluidized bed dynamics, although most theoretical model approaches fail to capture the details of the particle flow mechanics (Deen et al., 2007). Some recent developments reveals the importance of the coupling between gas and solid phase to successfully represent the physics behind the fluidized bed dynamics in pulsating flows (Wu et al., 2017) and the importance of distributor performance on the effectiveness of the fluidization (Kanholy et al., 2017). On the other hand, the discrete bubble model approach (Bokkers et al., 2006; Briongos et al., 2011; Pannala et al., 2004) tries to answer the long-term behavior of gas-solid fluidized beds by direct modeling the bubbling phenomena observed. However, in order to speed up the solution process and to focus on the long-term information, a better understanding of the bubble generation process to measure the distributor effect on the bed dynamics becomes crucial, having a significant impact on the computational cost of the bubble generation modelling.

In this work the windowed wavelet coherence method is applied to measure the correlation between the short-term dynamics characterizing the bubble generation at the distributor plate and the long-term dynamics due to the bubble pattern characterizing the stationary bed operation of different fluidized bed systems.

In order to analyze the effect of the distributor performance at different scales, the fluidized bed is operated with four different perforated plate distributor (with the same open area) with four different fixed bed height and at two relative gas velocity values.

2. Experimental setup and experimental techniques

The experimental setup for this work was similar to the one described in Sánchez-Delgado et al. (Sánchez-Delgado et al., 2013b). It consisted on a pseudo 2-D cold fluidized bed, made of glass with the rear wall covered in black to improve the contrast during the images acquisition,. The fluidized bed dimensions were 30 cm width (W), 150 cm height (H) and 0.5 cm thickness (t). Two spotlights were used for fluidized bed illumination and a Nikon 1 camera was used for the images acquisition at a frame rate of 60 fps for approximately 30 seconds. The bed material used was Ballotini glass spheres, previously sieved to a diameter range between 425 and 600 μm (Geldart B classification (Geldart, 1973)), with a particle density of $\rho_p = 2500\, kg/m^3$.Four different fixed bed heights were studied (h = 15, 30, 45 and 60 cm). Air was used as a fluidization agent, and the minimum fluidization velocities for each experiment were measured for the four bed heights, resulting $U_{mf} \approx 0.24\ cm/s$ for all cases. In addition, two different relative gas velocities were tested ($U_r = U/U_{mf}$ = 2 and 2.5) for each bed height.

Four different distributors (perforated plates) have been used during the experiments. The number and diameter of the holes, equally spaced along the distributor for each distributor, have been calculated to keep constant the open area value, ϕ =0.015, defined as the relation between the area of the holes and the horizontal section. Table 1, shows the holes characteristics for each distributor.

Distributor	Number of holes	Hole diameter, $d_o(mm)$
D06	6	2.2
D08	8	1.9
D20	20	1.2
D28	28	1

Table 1: Distributors characteristics

In order to avoid interactions between the bed and the air-supply system, the pressure drop through the distributors was experimentally determined, and compared with the bed pressure drop during the experiments, resulting in a no interaction between the bed and the air-supply system (Sasic et al., 2005, 2004). Figure 1 shows the characteristic curve for all the distributors. Considering the superficial gas velocities used in this research, from 0.48 to 0.60 m/s, it can be noted that the four perforate distributors had the same pressure drop.

Figure 1. Characteristics curves for the distributors defined in Table 1.

The combination of all these operation conditions results in 32 different cases which are summarized in Table 2, showing the nomenclature used in this work for each case.

h (cm)	*15*	*30*	*45*	*60*

U/U_{mf}	*2*	*2.5*	*2*	*2.5*	*2*	*2.5*	*2*	*2.5*
D06	1	2	3	4	5	6	7	8
D08	9	10	11	12	13	14	15	16
D20	17	18	19	20	21	22	23	24
D28	25	26	27	28	29	30	31	32

Table 2: Experimental conditions (distributor type, fixed bed height and excess gas) and experiment identification.

2.1 Applied techniques for image post-processing

The use of Digital Image Analysis (DIA) allows to characterize the dense and bubble phase in a pseudo-2D fluidized bed (Asegehegn et al., 2011; Bokkers et al., 2006; Busciglio et al., 2008; Garcia-Gutierrez et al., 2014; Gómez-Hernández et al., 2017; Julián et al., 2015; Sánchez-Delgado et al., 2010b, 2013b; Shen et al., 2004). A MATLAB algorithm transformed the gray scale images into binary images, allowing us to measure the concentration maps of solid phase, the freeboard height, the details of bubble generation, and the growth and interaction in the fluidized bed. The details of the code can be found in (Sánchez-Delgado et al., 2013b, 2010a). The average dynamics of the fluidized bed has been determined with this technique. In particular the DIA has been used to calculate:

-Mean value of freeboard height, h_{fb}: the freeboard height determination plays a crucial role in the study of the fluidized bed, since this parameter determinate the maximum height of the fluidized bed where the mean properties of solid and dense phases can be studied.

-Time averaged concentration maps, $\overline{C_{x,y}}$,: these maps reports information about the preferred bubble paths and the solid concentration regions (fraction of time that a certain point (x,y) is occupied by solids). The maps are calculated by means of the images superposition, according with a previous work of Sánchez-Delgado et al. (Sánchez-Delgado et al., 2013b).

-Mean bubble diameter evolution with height and mean value of numbers of bubbles with height, D_{eq} and N_{bm} respectively: the fluidized bed height was discretized in spaces of one centimeter, and in each space, the D_{eq} has been calculated as the mean of the bubbles diameters detected in each region. Besides, in the same spaces, the mean value of bubble presence has been also calculated. To avoid bubble interferences, a gap time of 20 images ($\Delta t = 1/3\ s$) has been defined prior to the image analysis.

-Evolution of Bubble Void Fraction (BVF) with time: the BVF represents the proportion of a certain Region Of Interest (ROI) occupied by bubble voids (Lim et al., 2007). The evolution of the BVF with time was generated by means of the DIA technique applied in every images of each case.

2.2 Wavelet Coherence Analysis (WCA)

After the application of the DIA technique to calculate the parameters described above, a wavelet coherence analysis has been used to study the dynamic of the fluidized bed at different scales.

Fluidized bed dynamics should be studied at different frequency scales. Moreover, such multiphase mixture of dynamics has their own time dependent physical processes. Traditional measures in time domain based on statistics over ensemble averages, cannot properly separate the dynamics characterizing the different scales. It is therefore needed a multiscale approach, to move the dynamic information to the time-frequency domain. Wavelet analysis can be used to successfully extract the local-frequency information in time from a signal. The wavelet transform makes an adaptive conversion to the time-frequency domain by using sliding windows of different sizes that moves over the measured signals. Since the basic functions of the wavelet are defined in both and frequency, it is possible to adapt the window size to improve the time resolution of both high frequencies and low frequencies. In this research, the continuous wavelet transform is used to analyze BVF time series. The Morlet wavelet is characterized by a Gaussian envelop, and therefore it is possible to define an adaptive window size to optimize in both the real and the Fourier spaces the time localization of the different high and low frequency components characterizing the measured BVF time series (Torrence and Compo, 1998; Torrence and Webster, 1999).

The idea of coherence when analyzing measured signals is viewed as measure of the degree of correlation between two time series or two representation of the measured time series to be compared (Labat, 2005). The coherence is defined as the square of the cross spectrum normalized by the individual power spectra (Grinsted et al., 2004).

$$R_n^2 = \frac{\left|S\left(s^{-1}W_n^{XY}(s)\right)\right|^2}{S\left(s^{-1}\left|W_n^X(s)\right|^2\right)\cdot S\left(s^{-1}\left|W_n^Y(s)\right|^2\right)} \qquad 1$$

Where W_n^{XY}denotes for the cross-wavelet spectrum, which is defined as $W_n^{XY}(s) = W_n^X(s)W_n^{Y*}(s)$, with $W_n^{Y*}(s)$ being the complex conjugate of the wavelet transform $W_n^Y(s)$. S is a smoothing operator which indicates averaging in time and in scale. Accordingly, the wavelet coherent coefficient is first averaged across time and then averaged across scales. For wavelet coherence analysis, the averaging process in time and scale is critical. Otherwise, nominator and denominator becomes equal and a value of unity should be found for any two compared processes (Maraun et al., 2007). In this work, following the procedure developed by Torrence and Wbster (Torrence and Webster, 1999), a smoothing in time was performed by a convolution with the absolute value of the wavelet. To average the value through the scales, the approach of presented by Grinsted et al. (Grinsted et al., 2004) was used. The number of scales to use in the wavelet transform was chosen, according to Torrence and Compo (Torrence and Compo, 1998), as a fractional power of two . As the continuous wavelet transform has edge artifacts, consequently, errors will occur at the beginning and at the end of wavelet power spectrum. The cone of influence COI in which the edge effect cannot be

ignored is plotted along with the result of the squared wavelet coherence (Mallat, 2009; Torrence and Compo, 1998). The size of the Cone Of Influence (COI) at each scale gives a measure of the decorrelation time. The statistical significance level of the wavelet coherence was estimated using Monte Carlo method. According to that, the refined Amplitude Adjusted Fourier Transform algorithm (AAFT) reported by Schreiber and Schmitz (Schreiber and Schmitz, 1996) was applied to produce surrogate data sets which have the same power spectrum and distribution that the measured time series. About 200 of surrogate data set pairs suffice to set and appropriate wavelet red noise background spectrum (Torrence and Compo, 1998). The wavelet coherence was computed for each pair. The local wavelet spectrum was then defined as the vertical slice of the wavelet coherence through all the scales at the time corresponding with the central value of the sampling interval. Once the background level was estimated, it was assumed that different realizations of the BVF time series will be randomly distributed about the expected background. According to that, the null hypothesis assumes that if a peak appearing in the wavelet spectrum is significantly above the background red noise, then it would correspond with a true dynamic feature with a 95% confident level. To establish the 95% confident level it was assumed that the background signals are stationary and therefore the value of the coherence function at the different scales do not change with time. Finally, the displacement of the oscillation phenomena characterizing the BVF time series serves, in this research, as a measure of the synchronization in terms of the local phase advance of coherent periodic component. According to that, the phase differences of the two time series compared each localizing time origin and scale are represented as arrows during the wavelet coherent analysis.

3. Results and discussion

The combination of the conventional DIA and the novel Wavelet Analysis techniques applied over the images acquired in the experiments, have allowed to study the effect of the distributor type, excess gas and the fixed bed height, in the bubble generation, growth and interaction within the fluidized bed. The results obtained during the analysis of the experiments involve two different approaches.

First, in order to study the distributor type and the operation conditions effects in the long term fluidized bed behavior, a conventional analysis (DIA) within a 2-D bubbling fluidized bed is presented to measure the bubble and dense phase bed behavior in terms of ensemble averages. In order to capture the features of the different scales visually observed during the tests, and to compare the effect of the distributor type, the superficial gas velocity and the fixed bed height, both the bubbles and the dense phase were analyzed in the region where bubbles are detected. According to that, the evolution of the numbers of bubbles and mean value of bubbles diameter with the height attained in each case was calculated. With regard to the dense phase, the time averaged solid concentration maps within the fluidized bed were also calculated.

Secondly, the evolution of the BVF with time is used to analyze in detail the bubble generation region. Accordingly, a ROI was defined in order to study the bubble generation in an specific window. Two different ROIs regions are explored by varying the window height above the jet region at 2 cm and 10 cm, in order to analyze the ROI influence in the results obtained by the Wavelet Coherence Analysis. The phase coherence of the BVF time series identified shared time-variability at some frequencies characterizing the long-term and short-term dynamics of the bed investigated. In order to characterize the characteristic frequencies of the BVF time series, the power spectrum (PSD) calculated following the well-known Welch's period gram method is used.

Conventional analysis: long term fluidized bed behavior

The region where the bubbles are detected along the bed, has been defined as the region comprised from the height just above the Jet Region (JR) to the freeboard height. The JR has been widely studied by many authors and it is defined as the region where the jet penetration takes place, widely studied by many authors (Agarwal et al., 2011a; Blake et al., 1990; Rees et al., 2006). In this work, the jet penetration length for all cases, was determined using the correlation presented by Blake et al. (Blake et al., 1990)

$$\frac{L}{d_o} = 55.6\left(\frac{V^2}{g d_o}\right)^{0.251}\left(\frac{\rho}{\rho_p}\right)^{0.322}\left(\frac{\rho^2 V d_p^2}{\mu d_o}\right)^{-0.134}$$

Where L (cm) is the jet length, V (cm/s) is the gas velocity in the orifice (approximately 32 cm/s and 40 cm/s, for cases of $U/U_{mf} = 2$ and 2.5 respectively), g (cm/s^2) is the gravitational acceleration, d_o (cm) is the orifice diameter, d_p (cm) is the particle diameter, ρ (g/cm^3) is the gas density, ρ_p (g/cm^3) is the particle density and μ ($g/cm \cdot s$) is the gas viscosity.

The freeboard height has been calculated for all cases as the average maximum height that particles reach in the fluidized bed, using the DIA technique (see Table 3).

h (cm)	*15*		*30*		*45*		*60*	
U/U_{mf}	*2*	*2.5*	*2*	*2.5*	*2*	*2.5*	*2*	*2.5*
D06	18.2	19.9	34.6	37.9	52.8	57.3	70.0	76.0
D08	17.7	19.1	35.7	38.1	53.7	58.6	68.8	73.7
D20	18.7	20.1	35.5	38.3	51.4	55.5	68.6	74.0
D28	19.1	20.7	36.0	38.1	50.6	54.7	69.2	74.1

Table 3: Freeboard height, h_{fb} (cm), for all cases.

As it can be observed, the freeboard height for different distributor, same fixed bed height (h) and excess gas (U/U_{mf}) does not present significant differences. Only the excess gas has a small effect on the freeboard height, when comparing cases with the same distributor type and the same fixed bed height.

Time averaged solid concentration maps

The averaged of the gas and solid flow patterns provides a picture of the bed structure characterizing the long-term dynamics of the fluidized bed system. Accordingly, when dealing with pseudo 2D fluidized beds, the time-averaged concentration maps give qualitative information about the internal structure of the gas solid fluidized bed related with the preferred bubble paths, dead zones and mixing regions. However, the averaged information of conventional analysis such as the time averaged concentration maps neglects time-dependent bed-distributor interactions, so the question regarding on how the distributor performance affects bed dynamics remain unanswered. Thus, in order to get insight in the bed structure for design and operation processes, the wavelet coherence analysis is used below complementary to the time averaged concentration maps to study the time-frequency location of the bed-distributor interactions.

Figure 2.1 and 2.2 show the distributor effect in the internal structure of the fluidized bed. Figure 2.1 shows the time averaged particle concentration maps, for cases 2, 10, 18 and 26 (h/W = 0.5, h = 15 cm, U/U_{mf} = 2.5) Similarly, Figure 2.2 shows the distributor effect in the internal structure of the bed for cases 8, 16, 24 and 32 (h/W = 2, h = 60 cm, U/U_{mf} = 2.5). In both figures, the solid line represents the freeboard height for each case, and the dash line represents the JR for each case.

a)

b)

c)

d)

Figure 2.1: Time averaged particle concentration map: a) case 2, b) case 10, c) case 18 and d) case 26. The solid line represents the freeboard height and the dashed-line represents the jet region height.

a)

b)

c)

d)

Figure 2.2: Time averaged particle concentration map: a) case 8, b) case 16, c) case 24 and d) case 32. The solid line represents the freeboard height and the dashed-line represents the jet region height.

As expected, the time averaged concentration maps characterizing the gas and solid flow circulation patterns of different beds, are affected by the fixed bed height. For cases with a low aspect ratio (Figure 2.1), the DIA provides a clear picture of the jet region, where it can be observed how as increasing the number of orifices (orifice

diameter decreases), the length jet penetration decreases (Rees et al., 2006), due to the decrease of the mass flow rate per orifice. Therefore, the gas is more uniformly distributed. In contrast, in Figure 2.2 (cases with the highest be aspect ratio) the effect of the distributor type in the internal structure of the fluidized bed is not clearly reflected by the measured time averaged concentration maps. In these cases, the observed effect of orifice number on better gas distribution can be recognized with less resolution. The fact the DIA technique loses resolution as increasing bed height, constrains the reliability of the information collected from those systems. Nevertheless, the averaged effect of the distributor can still be seen in the gas and solid flow circulation patterns, particularly in the jet region close to the distributor, as well as the bubble path crossing the bed in the midsection bounded by two recirculation regions close to the walls.

Excluding the jet region, where the distributor plays a role in the jet length (the smaller the number of holes, the higher the mass flow of the gas through the orifice, the higher the jet length), the internal structure of the fluidized bed is little affected by the distributor.

In order to obtain quantitative information about the particles concentration profile at different bed height, that helps to identify the distributor effects in the solid and gas flow preferred paths, Figure 3 is presented. In the same case as in Figure 2, it is divided into Figure 3.1 (cases 2, 10, 18, 28) for low aspect ratio (h=15 cm) and Figure 3.2 (8, 16, 24, 32) for high aspect ratio (h=60 cm), showing the solid concentrations profiles at different bed height, specifically at 25, 50 and 75 % of the freeboard height.

a)

b)

c)

Figure 3.1: Particle concentration profile for cases 2, 10, 18 and 26, at different bed heights (% of freeboard height): a) 25, b) 50 and c) 75.

a)

b)

c)

Figure 3.2: Particle concentration profile for cases 8, 16, 24 and 32, at different bed heights (% of freeboard height): a) 25, b) 50 and c) 75

For cases with low bed aspect ratios (Figure 3.1) and low number of holes in the distributor (D06 and D08, cases 2 and 10 respectively) the particle concentration profile is clearly affected in regions close the distributor (25% h_{fb}). Is in these regions where

the jet penetration effect promotes the dead zones, moving zones and the jetting zones, previously defined by Agarwal et al. (Agarwal et al., 2011b), and it can be clearly observed the saw profile due to the jet effect. However, once the distance to the distributor becomes higher (50-75% h_{fb}), the saw profile disappear and the particle concentration profile does not present significant differences with height. On the other hand, for cases 18 and 26 (D20 and D28 respectively), where the bed aspect ratio is equal than in cases 2 and 10, but the number of holes is significantly higher, the saw contour presented in cases 2 and 10 close de distributor is flattened out (Agarwal et al., 2011b) and the jet penetration effect is practically imperceptible. For all these cases (2, 10, 18 and 26) the solid concentration profile above the jet influence region, presents certain similarities.

In the cases with higher aspect ratio value, Figure 3.2, the jet region has a relevant influence in very close regions to the distributor; however, the jet penetration effect is practically imperceptible from the point of view of particle concentration profiles at higher height than the jet region. In these cases, the typical spatial bubble distribution within the fluidized bed can be appreciate, where the bubble coalescence effect generate a preferred bubble path in the middle of the bed, and two zones of high concentration particles in the wall, promoting two recirculating vortex (Sánchez-Delgado et al., 2013c; Werther and Molerus, 1973).

Bubble diameter and number of bubbles with height

Bubbles are the main mixing mechanism in the fluidized beds, therefore, the number, size and velocity of them is directly related with the mixing quality and mixing rate within the fluidized bed. Their nucleation, growing and interaction, define the internal structure of the fluidized bed, delimiting the bubble paths, mixing zones, dead zones… described in the section below. By means of DIA, the bubbles have been identified and analyzed in order to characterize the effect of the distributor performance, the fixed bed height and the excess gas in the bubble mean diameter with height.

Figure 4.1 shows an example of the results obtained, representing the evolution of the mean bubble diameter (D_{eq}), with height (y), for cases 7, 15, 23 and 31 (D06, D08, D20 and D28, respectively) with $h = 60\ cm$, and $U/U_{mf} = 2$.

Figure 4.1:Effect of the distributor type in the evolution of D_{eq} with height for cases 7, 15, 23 and 31 ($U/U_{mf} = 2$ and h=60 cm)

Figure 4.2: Effect of the fixed bed height in the evolution of D_{eq} with height for cases 10, 12, 14 and 16 (D08 and $U/U_{mf} = 2.5$)

As it can be observed, there are no significant differences for the evolution of the bubble mean diameter with height when the effect of the distributor type is studied (Figure 4.1). Figure 4.2 shows the effect of the fixed bed height in the evolution of the mean bubble diameter with height (Cases 10, 12, 14 and 16, with distributor D08 and $U/U_{mf} = 2.5$. No effect with the fixed bed height is observed during the evolution of the D_{eq} with height within the fluidized bed.

The higher differences, when the distributor performance effect is analyzed, can be appreciated in the cases with the smallest fixed bed height, due to the higher height occupied by the jet penetration in comparison with the fixed bed height, and even then the distributor has a slight effect. For all cases, when the height is close to 80% of the fixed bed height, the bubble mean diameter start to show a non-linear relation with height, and this effect is more remarkable for case with higher fixed bed height. The coalescence effect of the bubble during the ascent within the fluidized bed, and the freeboard effect, explains the non-lineal behavior of bubble with height in the upper part of the bed. On the other hand, the excess gas has a direct effect in the bubble mean diameter. As it can be expected, higher values of superficial gas velocity, promotes higher bubbles diameters.

Numbers of bubbles

Another effect of the distributor type within the fluidized bed is the mean value of the bubble presence at a certain height. Next figure, Figure 5 shows an example of the results obtained for the mean numbers of bubbles variation (N_{bm}) with height, y.

Figure 5. Effect of the distributor type and excess gas on the mean value of number of bubbles with height for a fixed bed height of $h = 60\ cm$.

As it can be seen in Figure 5, the number of bubbles reaches the maximum value in regions close the distributor and then, decreases with the distance to the distributor. This is because of the small bubbles generated close to the distributor coalesce with other bubbles as they ascend. This effect is observed independently of the excess gas, bed aspect ratio or distributor configuration. The number of holes in the distributor has a clear effect in the number of bubbles generated, where the distributor with more holes generate a higher numbers of bubbles. This effect is clearer in regions close to the distributor. It corresponds to the bubble generation mechanism in a perforated plate, where the more air injection the greater the number of bubbles generated.

The effect of the fixed bed height (h) in the number of bubbles evolution (N_{bm}) with height (y), has been also studied. Figure 6 shows the evolution of $N_{bm}$with height for cases 10, 12, 14 and 16 (h = 15, 30, 45 and 60 cm, respectively), with a same distributor type and excess gas for all cases (D08 and U/U_{mf} = 2.5).

Figure 6: Evolution of the mean value of number of bubbles (N_{bm}) with height for cases 10, 12, 14 and 16 (fixed bed height of 15, 30, 45 and 60 cm respectively), distributor D08 and $U/U_{mf} = 2.5$

As it can be observed, the fixed bed height has a significant effect in the evolution of the N_{bm}, only in a region really close to the distributor, just above the jet region, where the nucleation and growth prior to the bubbles interaction (coalescence) take place. The higher the fixed bed height, the lower the number of bubbles detected in these regions. The analysis of the numbers of bubbles, at higher height reveals that the fixed bed height has no effect in the evolution of N_{bm} with height.

Although the conventional time averaged analysis provides a picture of the internal structure of the bed, and a characterization of the bubble number and bubble size, two question are still needed to be addressed: i) How the excess gas does affect distributor-bed interaction in time and frequency domains?; ii) how the distributor design affects bubble generation and dynamics and consequently, the time averaged bubble pattern?

Wavelet Coherence Analysis (WCA)

In order to answer these questions, the WCA has been used to study the short-term dynamics during the bubble production and the long-term dynamics during the bubble interaction. The WCA has been applied over the temporal series of the BVF for each case, for two different ROI (W10 and W2, 10 cm and 2 cm above the jet region, respectively). In this sense, the effect of the ROI can be studied by means of the WCA. Figures 7.1 and 7.2 show an example of the sequence of snapshots for different cases and the BVF signal with time for these cases, respectively.

a)

b)

a)

b)

Figure 7.1) sequence of snapshots ($\Delta t = 1/60\ s$) analyzed with DIA technique with different ROI sizes (10 cm and 2 cm, a) and b) respectively) for case 32 (D28, h = 60 cm, U/U_{mf} = 2.5)

Figure 7.2) BVF evolution with time for different ROI sizes: a) 10 cm ROI, b) 2 cm ROI, for Case 32.

As it can be observed, the DIA technique applied over both ROI, Figure 7.1, reports different internal structures of BVF within the fluidized bed, depending on the ROI sized selected. Besides, the evolution of the BVF with time (Figure 7.2) also shows that there are clear differences between signals, being that signals the time series used during the wavelet coherence analysis. The mean frequency values have been determined by means of the Power Spectra Density (PSD) for cases 2, 10, 18 and 26 (same fixed bed height and excess gas, h=15 cm, U/Umf =2.5). W2 wide windows delimit the region of the bubble production process, while in W10 wide windows the bubble generation, growing and interaction processes take place. The corresponding power spectral analysis for W2 is shown in Figure 8.1 for the bubble generation process mean frequencies values which range between 3.5 and 4 Hz. In contrast, the W10 wide windows which come from averaging the dynamics over a larger region, and which cover up to 10 cm above the jet region is characterized by shorter mean frequencies ranging between 1.6 and 2 Hz (Figure 8.2). Those values are characteristic of the bubbling bed regime developed at those operation conditions.

a)

b)

Figure.8. PSD results for W2 and W10 (a and b respectively) in cases 2, 10, 18 and 26

In view of the results, the selected ROI to determinate the bubble generation frequency, has a significant effect. Therefore, as expected, for a proper analysis of the bubble generation frequency, the ROI should be selected in a region just above the Jet Region.

The WCA has been applied over the BVF series to carry out a more complete study, not only on the effect of the ROI selected, but also on effect of the distributor type in the bubble frequency generation. The results of the WCA are shown in Figure 9, comparing short-term dynamic phenomena originated during the bubble production process phenomena (W2) with long-term bubbling dynamics (W10), for each distributor type.

Figure 9: Wavelet Coherence Analysis, comparing different wide window, for all distributors, at the same fixed bed height (h=15cm) and same excess gas $U/U_{mf} = 2.5$

From the coherence analysis can be observed that the bubble production process, which is the result of the distributor performance, affects significantly the frequency region (1.6 Hz> fm > 2 Hz) corresponding with the bubbling regime promoted within the bed. Thus contoured regions which identify true matching, can be found even at frequencies down to 1 Hz that are related with the long term bed behavior. This distributor effect is observed regardless of the distributor type.

Similar results are observed when the Wavelet Coherence Analysis is applied for the cases operated with higher fixed bed height. Consequently, it can be generally concluded that the bed height does not affect the distributor-bed interaction in time and frequency domains. In view of the results obtained for the WCA for all cases, the coherence found between the short-term and long-term dynamics represented respectively by the bubble production process and the subsequent bubbling dynamics seems to be barely affected by the distributor type. Only the case of distributor D06 and h=15 cm, in Figure 9, exhibit coherence at very short-term behavior (near 0.3 Hz). As expected, this result of similar coherence behavior is in line with previous result reported in literature where the Coherent Output Power (Van Der Schaaf et al., 2002, 1998) was used to identify joint behavior propagated through fast traveling pressure waves due to bubble coalescence, bubble eruptions bed mass oscillation and gas flow, which in the end are the dynamical processes behind the BVF time series.

Though it has been clearly shown, through the coherence analysis, that the bed dynamics is affected by the distributor performance, the question about the role of the distributor design on such measured fluidization characteristics is still unsolved. The WCA is used below to compare, in time-frequency domain, the different distributor performance by means of analyzing the BVF time series collected from the jet region of the perforate plated having 6, 8 and 20 orifices respectively. Figure 10, shows a sequence of snapshots of the JR ($\Delta t = 1/60$ s) analyzed with DIA technique, for cases 2, 10 and 18 (h = 15 cm, U/U_{mf} = 2.5). The analysis of the BVF in the jet region of the distributor plate of 28 orifices is not used because of the low resolution of the measurement technique for measuring at the jet region at those conditions.

a)

b)

c)

Figure 10: Sequence of snapshots ($\Delta t = 1/60\ s$) of the Jet Region, analyzed with the DIA technique: a) case 2 (D06), b) case 10 (D08) and c) case18 (D20). h = 15 cm, U/U_{mf} = 2.5

As in previous analysis, the PSD has been calculated for these three BVF time series. The results obtained in this analysis have been shown in Figure 11.

Figure 11.1: Evolution of the BVF with time for the Jet Regions for cases 2 (D06), 10 (D08) and 18 (D20), h = 15 cm, U/U_{mf} = 2.5

Figure 11.2: PSD results for the Jet Regions for cases 2 (D06), 10 (D08) and 18 (D20), h = 15 cm, U/U_{mf} = 2.5

Figure 11.1 reveals similar time-scales characterizing the jet region of the three plates distributors compared. Moreover, Figure 11.2, the average frequency characteristics measured by the corresponding frequency spectrums confirm the similarities of the dynamics governing the three jet regions compared.

Figure 12 represents the coherence of the Jet Region between distributors, for cases 2, 10 and 18. The fact is that when those similarities are compared through the Wavelet Coherence Analysis the results are analogous for the three distributor investigated.

Figure 12: Comparison of the BVF in the Jet Region, between different distributors

It is remarkable the fact that most of the high frequency oscillation are in phase, exhibiting a high degree of synchronicity. Thus, in one hand it can be observed a high degree of coherence across the scales characterizing the jet regions produced by the different distributor plates to the extent that no clear differences can be distinguished by visual inspection of the spectrograms shown in Figure 12. On the other hand, Figure 6, shows the variation of the number of bubbles with height for all cases considered in this research. Therefore, apparently it is clear that the bubble distribution and the corresponding gas-solid motion (Figures 3.1 and 3.2) depend on distributor design. Thus, how can be solved this apparent controversy? Where the bubble and gas-solid distribution characterizing the different bed systems come from? An explanation for the different time-averaged bubble patterns measured in the different bed systems can be found when studying the bubble production at the ROI located at 2 cm height from the Jet Region. Figure 13 shows a detail of the ROI selected for this analysis.

Figure 13: Detail of ROI definition for case 12 (D08, $h = 30cm, U/U_{mf} = 2.5$)

The DIA technique has been applied over the images to obtain the location and the probability to find a bubble at a certain time along the distributor (N_b^*), also called Probability Density Function (PDF). For this analysis, and for all cases, only 1 in 20 images has been analyzed, and the width of the fluidized bed has been discretized in spaces of 0.5 cm along the distributor. The excess gas and the fixed bed height have been also studied to determine the effect of these operation conditions in the bubble generation mechanism. Figure 14.1 shows an example of the distributor effect in the PDF of bubble generation along the distributor, for cases with D8 and D20 , as well as the excess gas influence on it. On the other hand, Figure 14.2 shows the effect of the

fixed bed height in the PDF of bubble generation along the distributor, for cases with D06 and D28.

Figure 14.1: Distributor effect in the PDF of bubble generation along the distributor, for cases with D8 and D28, and the excess gas effect.

Figure 14.2: Distributor effect in the PDF of bubble generation along the distributor, for cases with D6 and D28, and the fixed bed height effect.

In view of the results of Figure 14.1, it can be clearly observed, that the distributors with low numbers of holes (cases 13 and 14 with D08, and cases 1, 3, 5 and 7 with D06), present a bubble production localized preferentially above the holes, with the maximum of the probability at the center of the corresponding orifices. In contrast, for cases where the bed is operated with higher number of holes in the distributor (cases 26, 28, 29, 30 and 32 with D28) the bubble generation spread out towards homogeneous distribution. Besides, Figure 14.1 shows that an increase of the excess gas for cases with low number of holes, promotes a smoothing of the saw profile of N_b^*, and the Figure 14.2 shows that the fixed bed height does not affect the profile of N_b^* along the distributor, for all the distributor types.

Therefore, though the time-frequency behavior of the different distributor plates exhibit a high coherence and synchronicity from the bubble production process point of view, the way in which the bubble generation takes place across the orifice plate (uniformly or intermittently distributed) give rise to the different time-averaged bubble and solid-gas flow pattern characterizing bed dynamics.

Conclusions

In the present work, two different techniques have been used to characterize the effects of the distributor and the operating conditions, in the bubble generation, growth and interaction, over the fluidized bed dynamics, in the short and long terms.

In view of the results obtained by means of the application of conventional techniques as Digital Image Analysis (DIA) and innovative techniques as Wavelet Analysis (WA), over the images acquired in the experiments, the following conclusions are described:

It can be concluded that for distributors with the same open area, and subsequently with the same relation between pressure loss through the distributor and the superficial gas velocity, the bubble generation mechanism does not affect the mean bubble behavior within the fluidized bed, or in other words, the distributor performance has no effect on the long term dynamic of the fluidized bed. More detailed studies in the bubble generation region (just above the Jet Region) conclude

that the distributor performance has no effect on the bubble generation frequencies. However, the results obtained regarding the Probability Density Function (PDF) of the bubbles distribution in the bubble generation region, reveals that the distributor performance has a direct effect on the locations of the bubble generation points along the distributor, being this the only region affected by the distributor performance, since from this area is not possible to distinguish the distributor type used, in terms of fluidized bed dynamics. Distributors with a greater number of holes, promote more homogenous PDF profiles along the distributor.

In terms of fixed bed height and excess gas, it can be conclude that the fixed bed height do not affect the PDF of bubbles in the bubble generation region, however, at higher values of the excess gas, the PDF of bubble distribution in the bubble generation region presents more homogenous distribution profiles.

These conclusions have a special relevance in the direct modelling of the bubbling phenomena, and the effect of it in the short-term and long-term behavior of gas-solid fluidized bed.

NOMENCLATURE

Δt: Time gap between images [s]

$\overline{C_{x,y}}$: Mean value of particle concentration in position x,y [-]

d_p: Particle diameter [μm]

d_o: Orifice diameter [mm]

D_{eq}: Equivalent diameter of bubble [cm]

f_m: mean bubbling frequency [Hz]

g: Gravitational acceleration [m/s^2]

h: Fixed bed height [cm]

h_{fb}: Freeboard height [cm]

H: Reactor height [cm]

L: Jet length [cm]

n: Localized time index, [-]

N_{bm}: Mean value of number of bubbles at certain height

N_b^*: probability to find a bubble at a certain time along the distributor [%]

R_n^2: Degree of correlation between series

s: Wavelet scale.

t: Fluidized bed thick [cm]

U: Superficial gas velocity [cm/s]

U_{mf}: Minimum fluidization velocity [cm/s]

U_r: Relative gas velocity [-]

V: Gas velocity per orifice [cm/s]

W: Fluidized bed width [cm]

W_n^{XY}: Cross wavelet spectrum

$W_n^{Y*}(s)$: Continuous wavelet transform

x: Horizontal position [cm]

X: Time series compared.

y: Vertical position [cm]

Y: Time series compared.

Greek symbols

ρ_p: Particle density [g/cm^3]

ρ: Gas density [g/cm^3]

φ: Open Area

μ: Gas viscosity [g/cm]

This research did not receive any specific grant from funding agencies in the public, commercial, or not-for-profit sectors.

APPENDIX

Wavelet analysis

The wavelet coherence analysis used through this research applies the fast Fourier transform algorithm according to the methodology reported in (Torrence and Compo, 1998). Thus the continuous wavelet transform, $W_n(s)$, is computed as the inverse

transform of the product between the Discrete Fourier transform, DFT, of the BVF time series and the complex conjugate of the wavelet function $\hat{\psi}(s\omega_k)$

$$W_n(s) = \sum_{k=0}^{N-1} \hat{x}_k \hat{\psi}^*(s\omega_k) e^{i\omega_k n \delta t},$$

Where the wavelet function and the DFT read as:

$$\hat{\psi}(s\omega_k) = \left(\frac{2\pi s}{\delta t}\right)^{1/2} \pi^{-1/4} H(\omega) e^{-(s\omega-\omega_0)^2/2}$$

$$\hat{x}_k = \frac{1}{N} \sum_{k=0}^{N-1} x_n \, e^{-2\pi i k n/N}$$

$H(\omega)$ stand for the Headviside step function, ω is the angular frequency, n is the localized time index, s the scale and δt the sampling step. Once the continuous wavelet transform has been obtained, the cross-wavelet spectrum is defined as $W_n^{XY}(s) = W_n^X(s) W_n^{Y*}(s)$, with $W_n^{Y*}(s)$ being the complex conjugate of the wavelet transform $W_n^Y(s)$. In order to solve equation 1, both the numerator and denominator are first averaged across times and then averaged across scales following [34] and then the coherence is given by solving equation 1.

References

Adánez, J., Abad, A., Mendiara, T., Gayán, P., de Diego, L.F., García-Labiano, F., 2018. Chemical looping combustion of solid fuels. Prog. Energy Combust. Sci. 65, 6–66. doi:10.1016/j.pecs.2017.07.005

Agarwal, G., Lattimer, B., Ekkad, S., Vandsburger, U., 2011a. Influence of multiple gas inlet jets on fluidized bed hydrodynamics using Particle Image Velocimetry and Digital Image Analysis. Powder Technol. 214, 122–134. doi:10.1016/j.powtec.2011.08.002

Agarwal, G., Lattimer, B., Ekkad, S., Vandsburger, U., 2011b. Influence of multiple gas inlet jets on fluidized bed hydrodynamics using Particle Image Velocimetry and Digital Image Analysis. Powder Technol. 214, 122–134. doi:10.1016/j.powtec.2011.08.002

Asegehegn, T.W., Schreiber, M., Krautz, H.J., 2011. Investigation of bubble behavior in fluidized beds with and without immersed horizontal tubes using a digital image analysis technique. Powder Technol. 210, 248–260. doi:10.1016/j.powtec.2011.03.025

Bakshi, A., Ghoniem, A.F., Altantzis, C., 2017. Mixing dynamics in bubbling fluidized beds. AIChE J. 63, 4316–4328. doi:10.1002/aic.15801

Blake, T.R., Webb, H., Sunderland, P.B., 1990. The nondimensionalization of equations describing fluidization with application to the correlation of jet penetration height.

Chem. Eng. Sci. 45, 365–371. doi:10.1016/0009-2509(90)87022-K

Bokkers, G.A., Laverman, J.A., van Sint Annaland, M., Kuipers, J.A.M., 2006. Modelling of large-scale dense gas-solid bubbling fluidised beds using a novel discrete bubble model. Chem. Eng. Sci. 61, 5590–5602. doi:10.1016/j.ces.2006.04.009

Briens, C.L., Briens, L.A., Hay, J., Hudson, C., Margaritis, A., 1997. Hurst's Analysis to Detect Minimum Fluidization and Gas Maldistribution in Fluidized Beds. AIChE J. 43, 1904–1908. doi:10.1002/aic.690430725

Briongos, J.V., Sanchéz-Delgado, S., Acosta-Iborra, A., Santana, D., 2011. A novel approach for modeling bubbling gas-solid fluidized beds. AIChE J. 57, 1733–1750. doi:10.1002/aic.12375

Busciglio, A., Vella, G., Micale, G., Rizzuti, L., 2008. Analysis of the bubbling behaviour of 2D gas solid fluidized beds Part I . Digital image analysis technique. Chem. Eng. J. 140, 398–413. doi:10.1016/j.cej.2007.11.015

Chen, L., Yang, X., Li, G., Yang, J., Wen, C., Li, X., Snape, C., 2017. Dynamic modelling of fluidisation in gas-solid bubbling fluidised beds. Powder Technol. 322, 461–470. doi:10.1016/j.powtec.2017.09.039

Clemson, P., Lancaster, G., Stefanovska, A., 2016. Reconstructing Time-Dependent Dynamics. Proc. IEEE. doi:10.1109/JPROC.2015.2491262

Deen, N.G., Van Sint Annaland, M., Van der Hoef, M. a., Kuipers, J. a M., 2007. Review of discrete particle modeling of fluidized beds. Chem. Eng. Sci. 62, 28–44. doi:10.1016/j.ces.2006.08.014

Donoho, D.L., Johnstone, I.M., 1995. Adapting to unknown smoothness via wavelet shrinkage. J. Am. Stat. Assoc. 90, 1200–1224. doi:10.1080/01621459.1995.10476626

Eow, J.S., Zhang, B., Ghadiri, M., 2003. Flow maldistribution and corner fluidisation in non-uniform packed beds: Pressure and velocity profiles. Powder Technol. 138, 169–188. doi:10.1016/j.powtec.2003.09.006

Garcia-Gutierrez, L.M., Soria-Verdugo, A., Marugán-Cruz, C., Ruiz-Rivas, U., 2014. Simulation and experimental study on the motion of non-reacting objects in the freeboard of a fluidized bed. Powder Technol. 263, 112–120. doi:10.1016/j.powtec.2014.04.085

Geldart, D., 1973. Types of gas fluidization. Powder Technol. 7, 285–292. doi:10.1016/0032-5910(73)80037-3

Geldart, D., Baeyens, J., 1985. The design of distributors for gas-fluidized beds. Powder Technol. 42, 67–78. doi:10.1016/0032-5910(85)80039-5

Gómez-Hernández, J., Sánchez-Delgado, S., Wagner, E., Mudde, R.F., van Ommen, J.R., 2017. Characterization of TiO2 nanoparticles fluidization using X-ray imaging and pressure signals. Powder Technol. 316, 446–454. doi:10.1016/j.powtec.2016.11.068

Grinsted, A., Moore, J.C., Jevrejeva, S., 2004. Application of the cross wavelet transform and wavelet coherence to geophysical time series. Nonlinear Process. Geophys. 11, 561–566. doi:10.5194/npg-11-561-2004

Haron, N.S., Zakaria, J.H., Mohideen Batcha, M.F., 2017. Recent advances in fluidized bed drying, in: IOP Conference Series: Materials Science and Engineering. doi:10.1088/1757-899X/243/1/012038

He, Y.-J., Wang, J.-D., Cao, Y.-J., Yang, Y.-R., 2009. Resolution of structure characteristics of AE signals in multiphase flow system - From data to information. AIChE J. 55, 2563–2577. doi:10.1002/aic

Helmi, A., Campos Velarde, I., Galluci, F., Van Sint Annaland, M., 2018. Hydrodynamics of dense gas-solid fluidized beds with immersed vertical membranes using an endoscopic-laser PIV/DIA technique. Chem. Eng. Sci. 182, 146–161.

Julián, I., Gallucci, F., van Sint Annaland, M., Herguido, J., Menéndez, M., 2015. Hydrodynamic study of a Two-Section Two-Zone Fluidized Bed Reactor with an immersed tube bank via PIV/DIA. Chem. Eng. Sci. 134, 238–250. doi:10.1016/j.ces.2015.05.009

Kanholy, S.K., Estejab, B., Battaglia, F., 2017. Modeling multiple gas jet interactions during fluidization in a pseudo-2D bed. Chem. Eng. J. 328, 1009–1021. doi:10.1016/j.cej.2017.07.116

Labat, D., 2005. Recent advances in wavelet analyses: Part 1. A review of concepts. J. Hydrol. doi:10.1016/j.jhydrol.2005.04.003

Lau, Y.M., Sujatha, K.T., Gaeini, M., Deen, N.G., Kuipers, J.A.M., 2013. Experimental study of the bubble size distribution in a pseudo-2D bubble column. Chem. Eng. Sci. 98, 203–211. doi:10.1016/j.ces.2013.05.024

Laverman, J.A., Roghair, I., Annaland, M.V.S., Kuipers, H., 2008. GAS-SOLID FLUIDIZED BEDS USING PARTICLE IMAGE VELOCIMETRY COUPLED WITH DIGITAL IMAGE. Chem. Eng. 86.

Li, G., Liu, Z., Feng, R., Jiao, W., Fang, Y., Wang, Z., 2018. Conceptual design and analysis of a novel system based on ash agglomerating fluidized bed gasification for co-production of hydrogen and electricity. Int. J. Hydrogen Energy. doi:10.1016/j.ijhydene.2017.12.049

Li, Y., Rong, J., Zhang, K., Fan, X., 2018. Impact of solid and gas flow patterns on solid mixing in bubbling fluidized beds. Chem. Eng. Res. Des. 132, 1037–1053.

Lim, C.N., Gilbertson, M. a., Harrison, a. J.L., 2007. Bubble distribution and behaviour in bubbling fluidised beds. Chem. Eng. Sci. 62, 56–69. doi:10.1016/j.ces.2006.08.034

Lombardi, G., Pagliuso, J.D., Goldstein, L., 1997. Performance of a tuyere gas distributor. Powder Technol. 94, 5–14. doi:10.1016/S0032-5910(97)03256-7

Lu, X., Li, H., 1999. Wavelet analysis of pressure fluctuation signals in a bubbling fluidized bed. Chem. Eng. J. 75, 113–119. doi:10.1016/S1385-8947(99)00097-2

Mallat, S., 2009. A Wavelet Tour of Signal Processing, A Wavelet Tour of Signal Processing. doi:10.1016/B978-0-12-374370-1.X0001-8

Maraun, D., Kurths, J., Holschneider, M., 2007. Nonstationary Gaussian processes in

wavelet domain: Synthesis, estimation, and significance testing. Phys. Rev. E - Stat. Nonlinear, Soft Matter Phys. 75. doi:10.1103/PhysRevE.75.016707

Marwan, N., Carmen Romano, M., Thiel, M., Kurths, J., 2007. Recurrence plots for the analysis of complex systems. Phys. Rep. doi:10.1016/j.physrep.2006.11.001

Maurer, S., Gschwend, D., Wagner, E.C., Schildhauer, T.J., Ruud van Ommen, J., Biollaz, S.M.A., Mudde, R.F., 2016. Correlating bubble size and velocity distribution in bubbling fluidized bed based on X-ray tomography. Chem. Eng. J. 298, 17–25. doi:10.1016/j.cej.2016.02.012

Pannala, S., Daw, C.S., Halow, J.S., 2004. Dynamic interacting bubble simulation (DIBS): an agent-based bubble model for reacting fluidized beds. Chaos 14, 487–98. doi:10.1063/1.1752181

Qureshi, A.E., Creasy, D.E., 1979. Fluidised bed gas distributors. Powder Technol. 22, 113–119. doi:10.1016/0032-5910(79)85013-5

Rees, a, Davidson, J., Dennis, J., Sfennell, P., Gladden, L., Hayhurst, a, Mantle, M., Muller, C., Sederman, a, 2006. The nature of the flow just above the perforated plate distributor of a gas-fluidised bed, as imaged using magnetic resonance. Chem. Eng. Sci. 61, 6002–6015. doi:10.1016/j.ces.2006.05.006

Sánchez-Delgado, S., Marugán-Cruz, C., Acosta-Iborra, a., Santana, D., 2010a. Dense-phase velocity fluctuation in a 2-D fluidized bed. Powder Technol. 200, 37–45. doi:10.1016/j.powtec.2010.02.005

Sánchez-Delgado, S., Marugán-Cruz, C., Acosta-Iborra, A., Santana, D., 2010b. Dense-phase velocity fluctuation in a 2-D fluidized bed. Powder Technol. 200, 37–45. doi:10.1016/j.powtec.2010.02.005

Sánchez-Delgado, S., Marugán-Cruz, C., Soria-Verdugo, a., Santana, D., 2013a. Estimation and experimental validation of the circulation time in a 2D gas-solid fluidized beds. Powder Technol. 235, 669–676. doi:10.1016/j.powtec.2012.11.012

Sánchez-Delgado, S., Marugán-Cruz, C., Soria-Verdugo, a., Santana, D., 2013b. Estimation and experimental validation of the circulation time in a 2D gas – solid fluidized beds. Powder Technol. 235, 669–676. doi:10.1016/j.powtec.2012.11.012

Sánchez-Delgado, S., Marugán-Cruz, C., Soria-Verdugo, a., Santana, D., 2013c. Estimation and experimental validation of the circulation time in a 2D gas-solid fluidized beds. Powder Technol. 235, 669–676. doi:10.1016/j.powtec.2012.11.012

Sánchez-Prieto, J., Soria-Verdugo, A., Briongos, J. V., Santana, D., 2014. The effect of temperature on the distributor design in bubbling fluidized beds. Powder Technol. 261, 176–184. doi:10.1016/j.powtec.2014.04.035

Sasic, S., Johnsson, F., Leckner, B., 2004. Interaction between a Fluidized Bed and Its Air-Supply System: Some Observations. Ind. Eng. Chem. Res. 43, 5730–5737. doi:10.1021/ie049763b

Sasic, S., Leckner, B., Johnsson, F., 2005. Fluctuations and waves in fluidized bed systems: The influence of the air-supply system. Powder Technol. 153, 176–195. doi:10.1016/j.powtec.2005.03.012

Sathiy Amoorthy, D., Sridhar Rao, C., 1979. Multi-orifice plate distributors in gas fluidised beds - a model for design of distributors. Powder Technol. 24, 215–223. doi:10.1016/0032-5910(79)87038-2

Sathiyamoorthy, D., Horio, M., 2003. On the influence of aspect ratio and distributor in gas fluidized beds. Chem. Eng. J. 93, 151–161. doi:10.1016/S1385-8947(02)00257-7

Sathiyamoorthy, D., Sridhar Rao, C., 1981. The choice of distributor to bed pressure drop ratio in gas fluidised beds. Powder Technol. 30, 139–143. doi:10.1016/0032-5910(81)80006-X

Sathiyamoorthy, D., Sridhar Rao, C., 1978. Gas distributor in fluidised beds. Powder Technol. 20, 47–52. doi:10.1016/0032-5910(78)80007-2

Saxena, S.C., Chatterjee, A., Patel, R.C., 1979. Effect of distributors on Gas-Solid Fluidization. Powder Technol. 22, 191–198. doi:10.1016/0032-5910(79)80026-1

Schreiber, T., Schmitz, A., 1996. Improved surrogate data for nonlinearity tests. Phys. Rev. Lett. 77, 635–638. doi:10.1103/PhysRevLett.77.635

Shen, L., Johnsson, F., Leckner, B., 2004. Digital image analysis of hydrodynamics two-dimensional bubbling fluidized beds. Chem. Eng. Sci. 59, 2607–2617. doi:10.1016/j.ces.2004.01.063

Sobrino, C., Acosta-Iborra, a., Santana, D., de Vega, M., 2009a. Bubble characteristics in a bubbling fluidized bed with a rotating distributor. Int. J. Multiph. Flow 35, 970–976. doi:10.1016/j.ijmultiphaseflow.2009.04.005

Sobrino, C., Almendros-Ibáñez, J.A., Santana, D., Vázquez, C., de Vega, M., 2009b. Maximum entropy estimation of the bubble size distribution in fluidized beds. Chem. Eng. Sci. 64, 2307–2319. doi:10.1016/j.ces.2009.01.046

Thorpe, R.B., Davidson, J.F., Pollitt, M., Smith, J., 2002. Maldistribution in Fluidized Beds. Ind. Eng. Chem. Res. 41, 5878–5889. doi:10.1021/ie0203173

Torrence, C., Compo, G.P., 1998. A Practical Guide to Wavelet Analysis. Bull. Am. Meteorol. Soc. 79, 61–78. doi:10.1175/1520-0477(1998)079<0061:APGTWA>2.0.CO;2

Torrence, C., Webster, P.J., 1999. Interdecadal changes in the ENSO-monsoon system. J. Clim. 12, 2679–2690. doi:10.1175/1520-0442(1999)012<2679:ICITEM>2.0.CO;2

Van Der Schaaf, J., Schouten, J.C., Johnsson, F., Van Den Bleek, C.M., 2002. Non-intrusive determination of bubble and slug length scales in fluidized beds by decomposition of the power spectral density of pressure time series. Int. J. Multiph. Flow 28, 865–880. doi:10.1016/S0301-9322(01)00090-8

Van Der Schaaf, J., Schouten, J.C., Van Den Bleek, C.M., 1998. Origin, propagation and attenuation of pressure waves in gas-solid fluidized beds. Powder Technol. 95, 220–233. doi:10.1016/S0032-5910(97)03341-X

Villa Briongos, J., Aragón, J.M., Palancar, M.C., 2006. Phase space structure and multi-resolution analysis of gas-solid fluidized bed hydrodynamics: Part I - The EMD approach. Chem. Eng. Sci. 61, 6963–6980. doi:10.1016/j.ces.2006.07.023

Walker, B. V., 1975. The effect of distributor type on conversion in a bubbling fluidised bed. Chem. Eng. J. 9, 49–61. doi:10.1016/0300-9467(75)88004-X

Werther, J., Molerus, O., 1973. The local structure of gas fluidized beds—II. The spatial distribution of bubbles. Int. J. Multiph. Flow 1, 123.138. doi:http://dx.doi.org/10.1016/0301-9322(73)90008-6

Wu, K., de Martín, L., Coppens, M.O., 2017. Pattern formation in pulsed gas-solid fluidized beds – The role of granular solid mechanics. Chem. Eng. J. 329, 4–14. doi:10.1016/j.cej.2017.05.152

Zunino, L., Pérez, D.G., Garavaglia, M., Rosso, O.A., 2007. Wavelet entropy of stochastic processes. Phys. A Stat. Mech. its Appl. 379, 503–512. doi:10.1016/j.physa.2006.12.057

Figure
Click here to download Figure: Figure1.eps

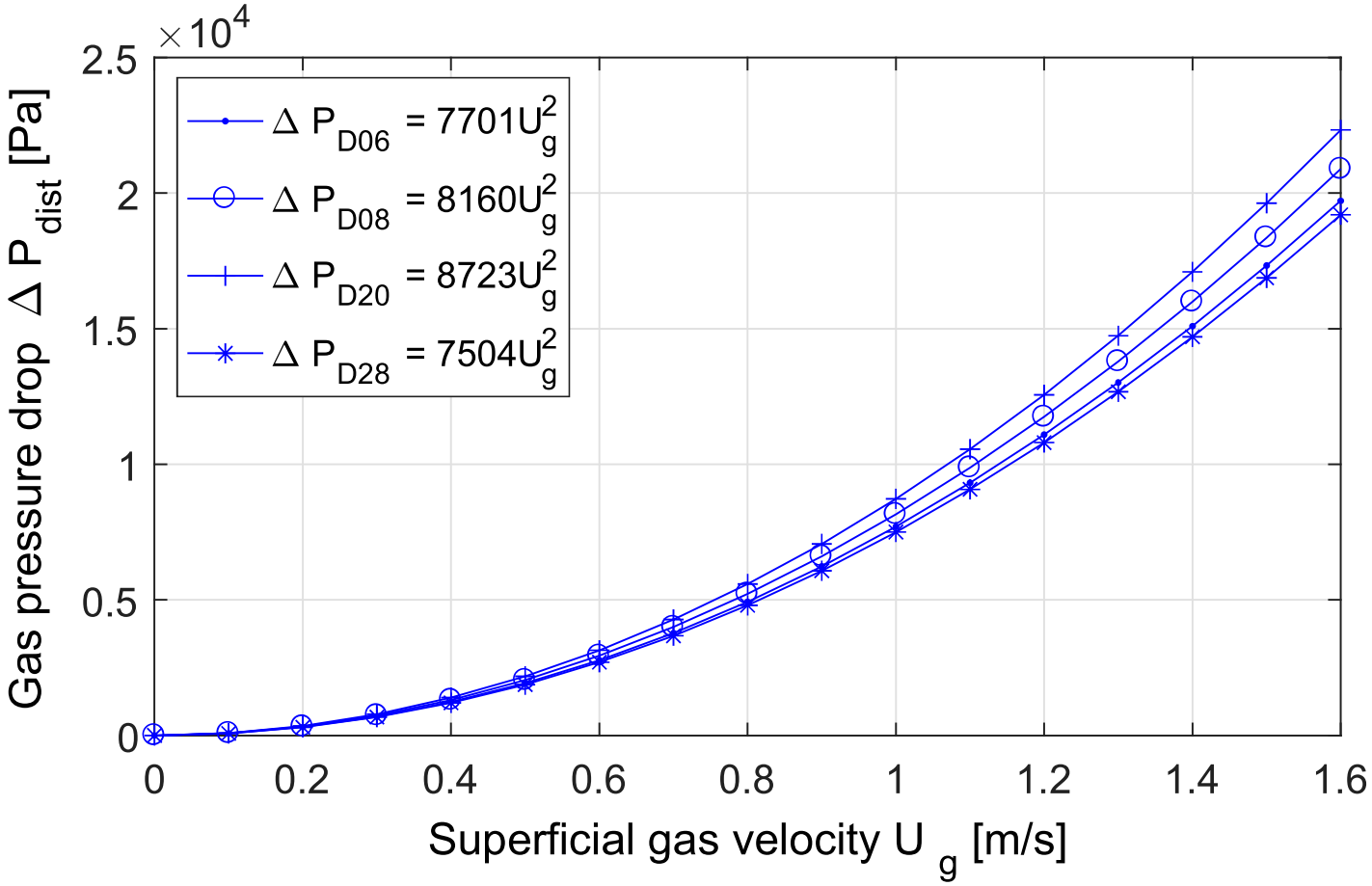

Figure
Click here to download Figure: Figure2_1_a.eps

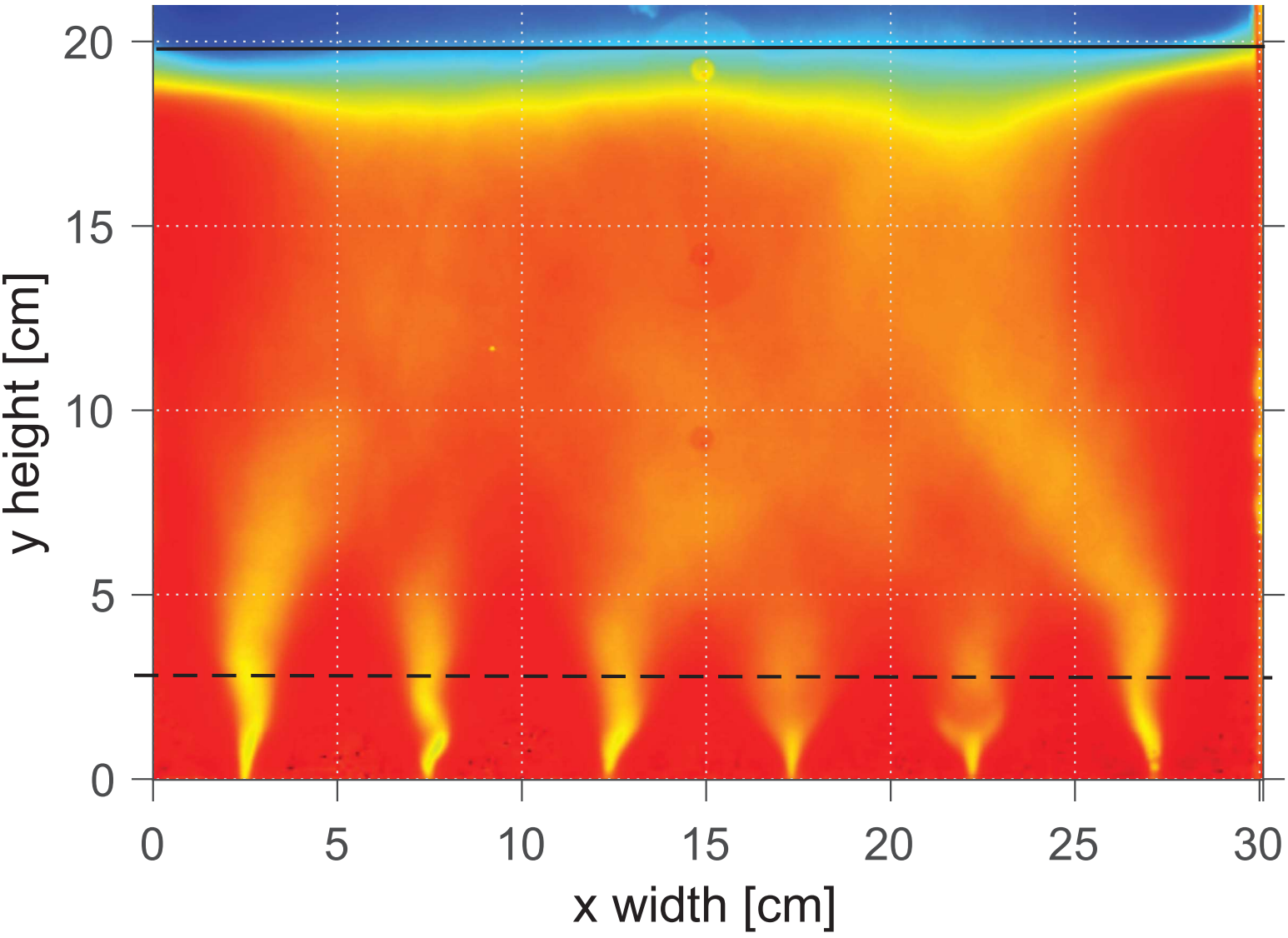

Figure
Click here to download Figure: Figure2_1_b.eps

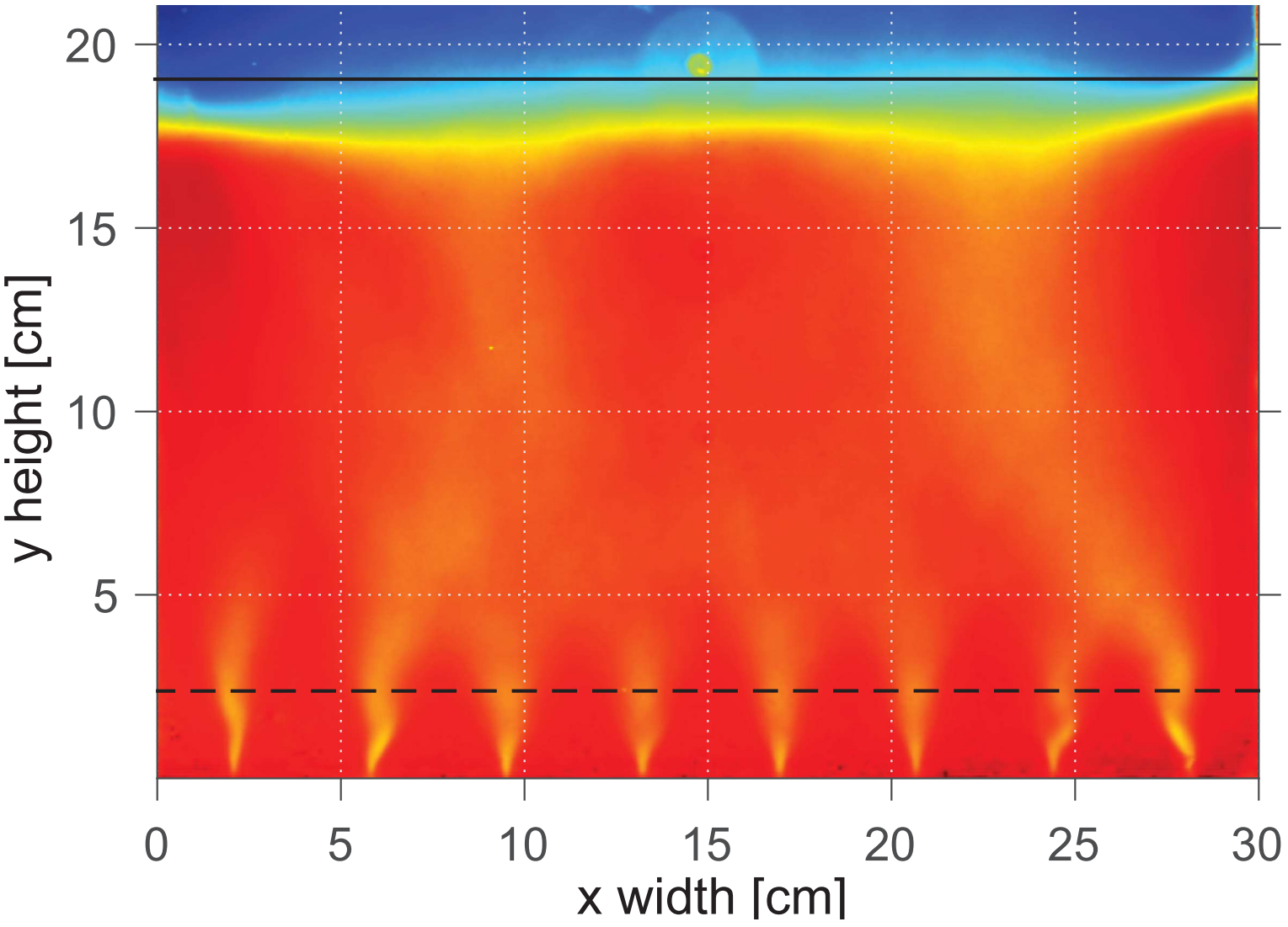

Figure
Click here to download Figure: Figure2_1_c.eps

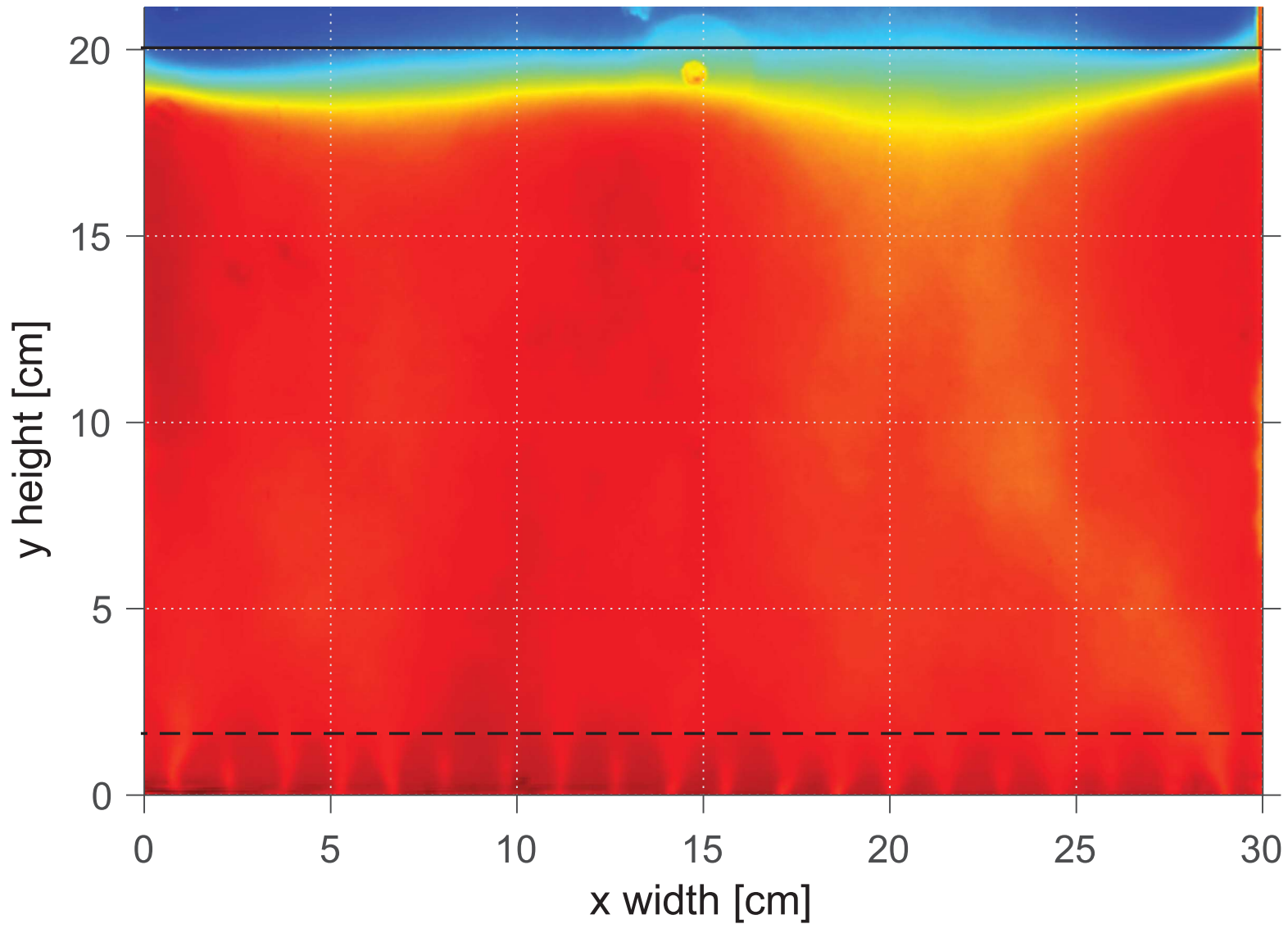

Figure
Click here to download Figure: Figure2_1_d.eps

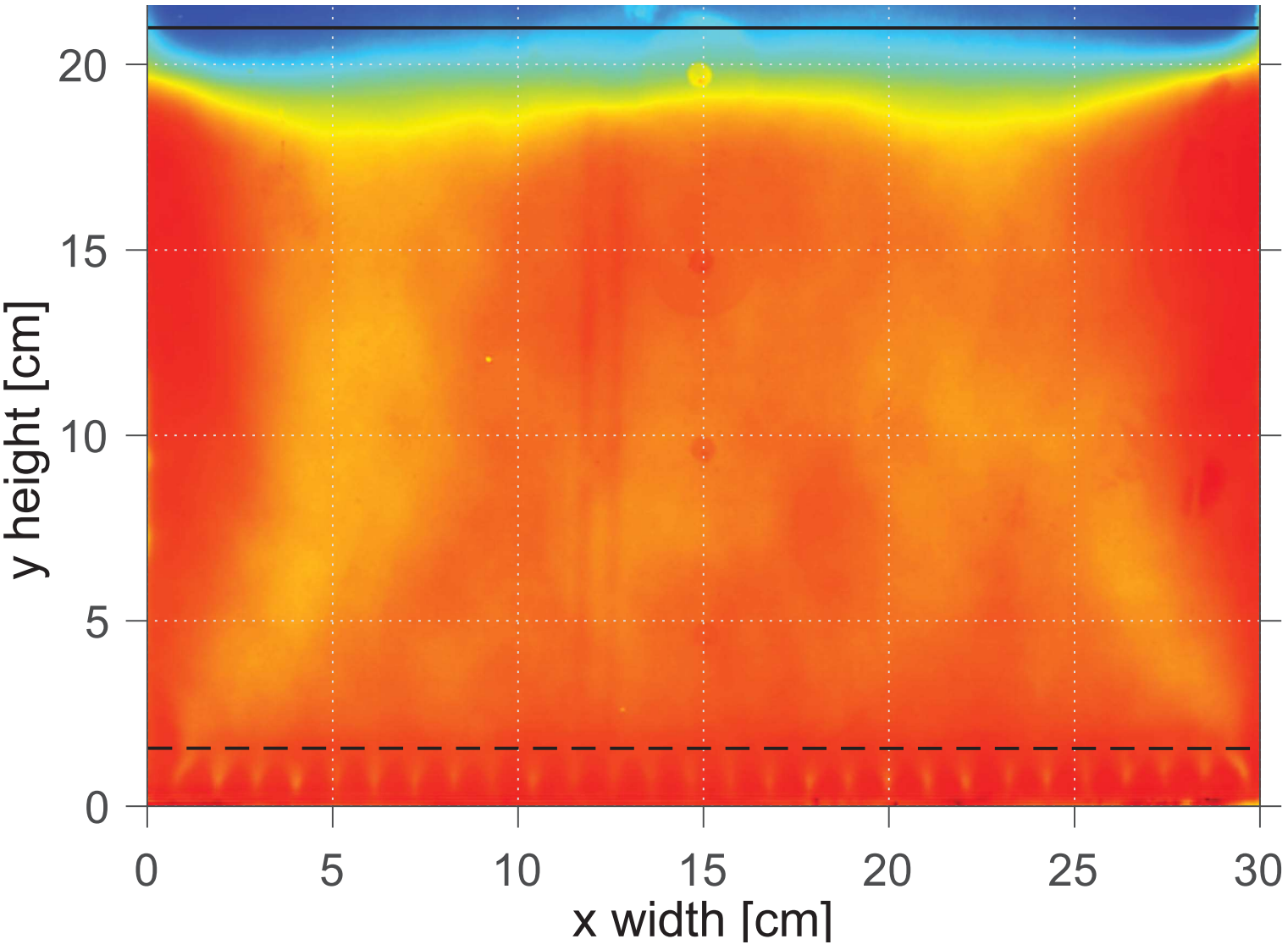

Figure
Click here to download Figure: Figure2_2_a.eps

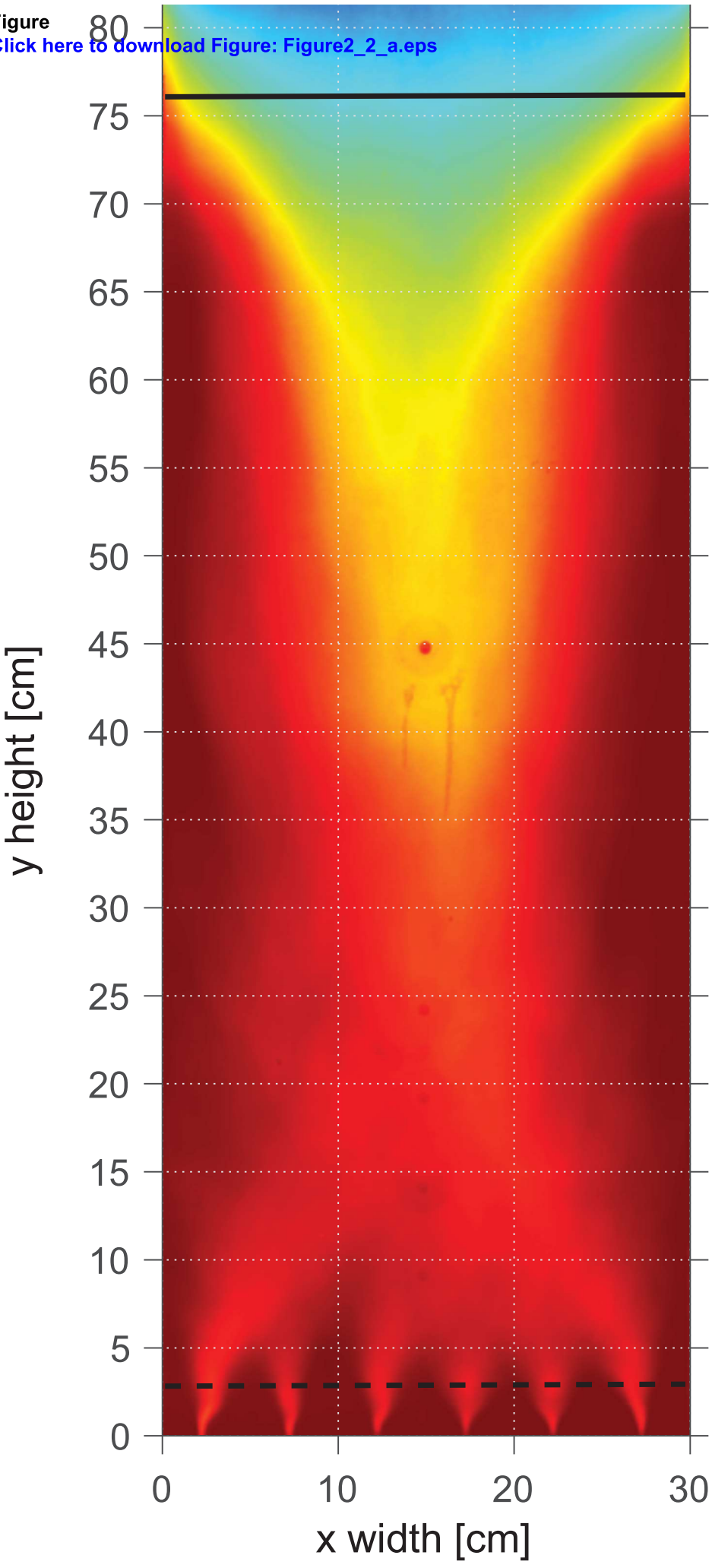

Figure
Click here to download Figure: Figure2_2_b.eps

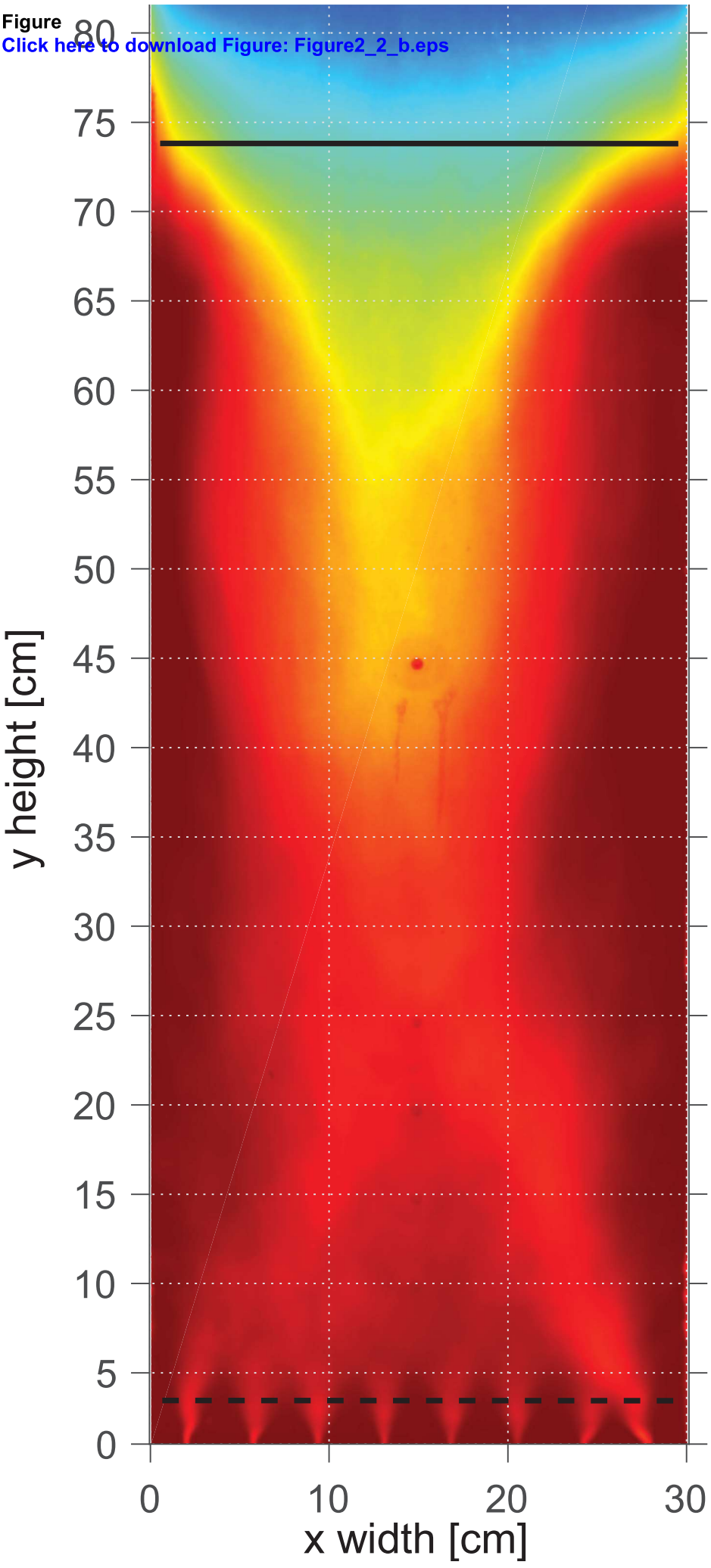

Figure
Click here to download Figure: Figure2_2_c.eps

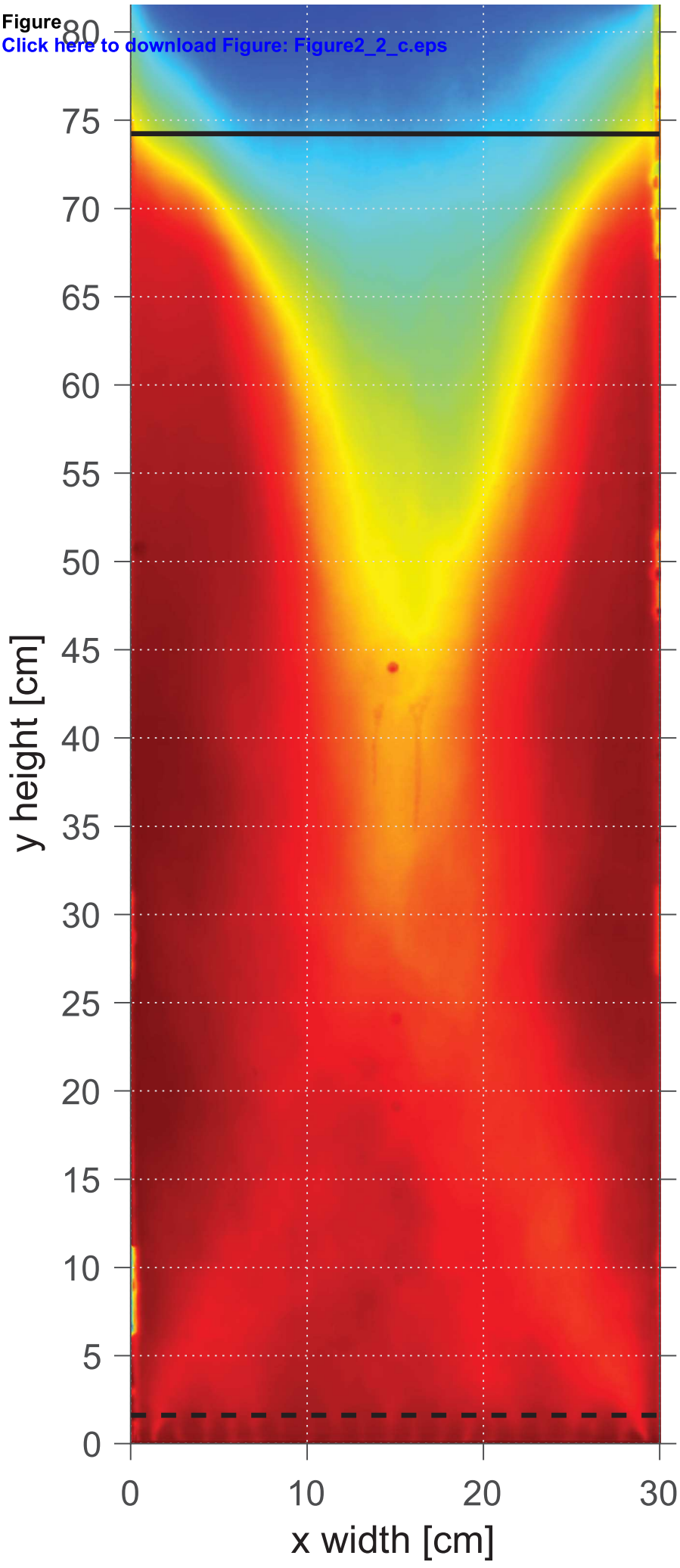

Figure
Click here to download Figure: Figure2_2_d.eps

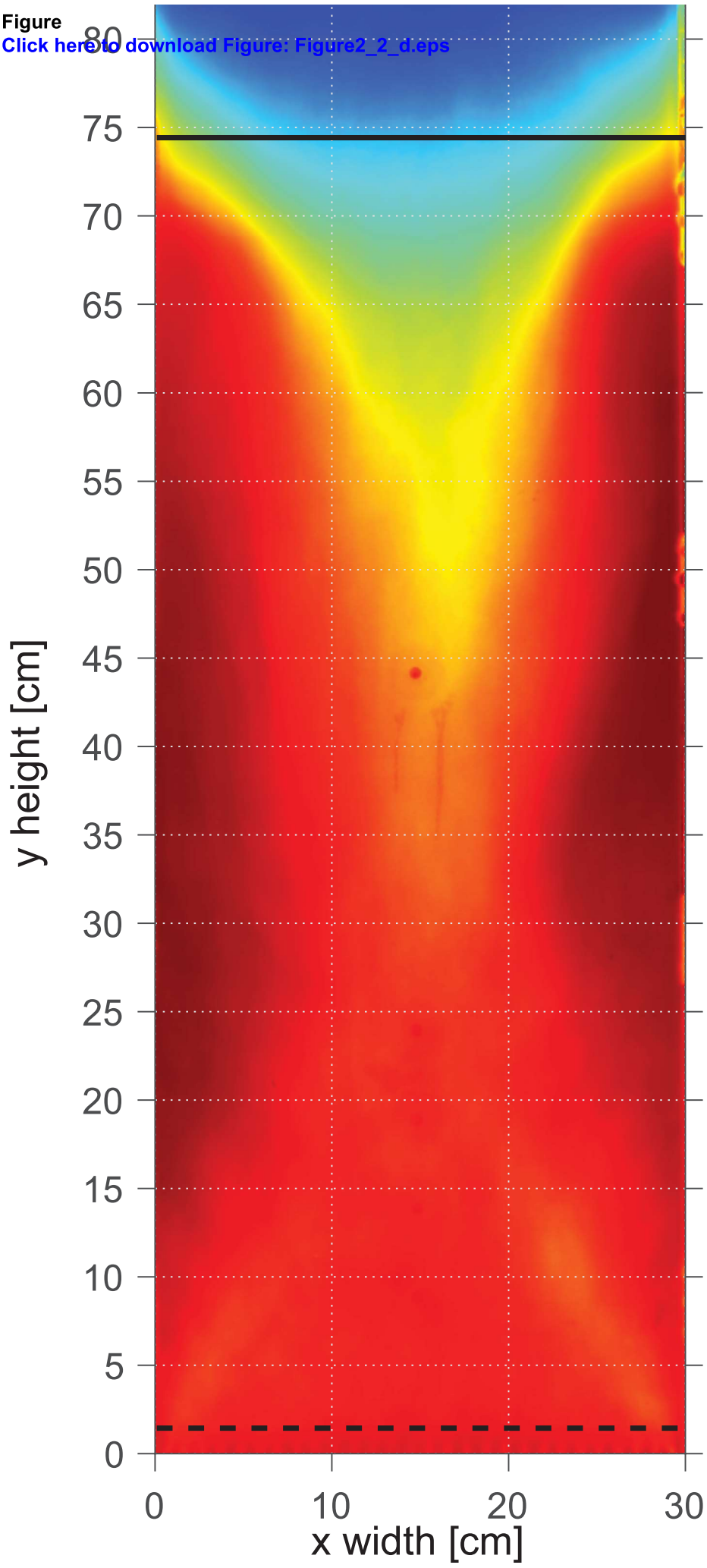

Figure

Click here to download Figure: Colorbar_Figure_2_1.eps

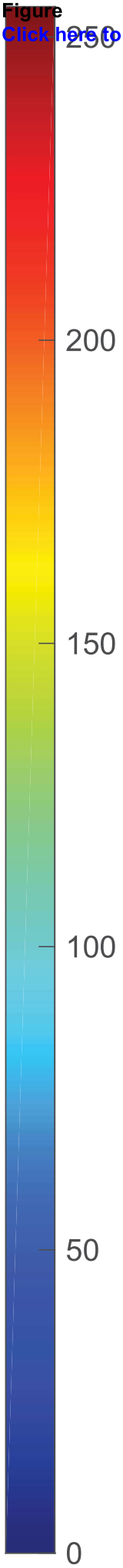

Figure

Click here to download Figure: Colorbar_Figure_2_2.eps

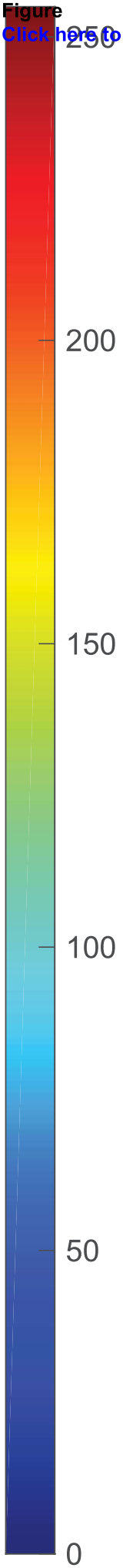

Figure
Click here to download Figure: Figure3_1_a.eps

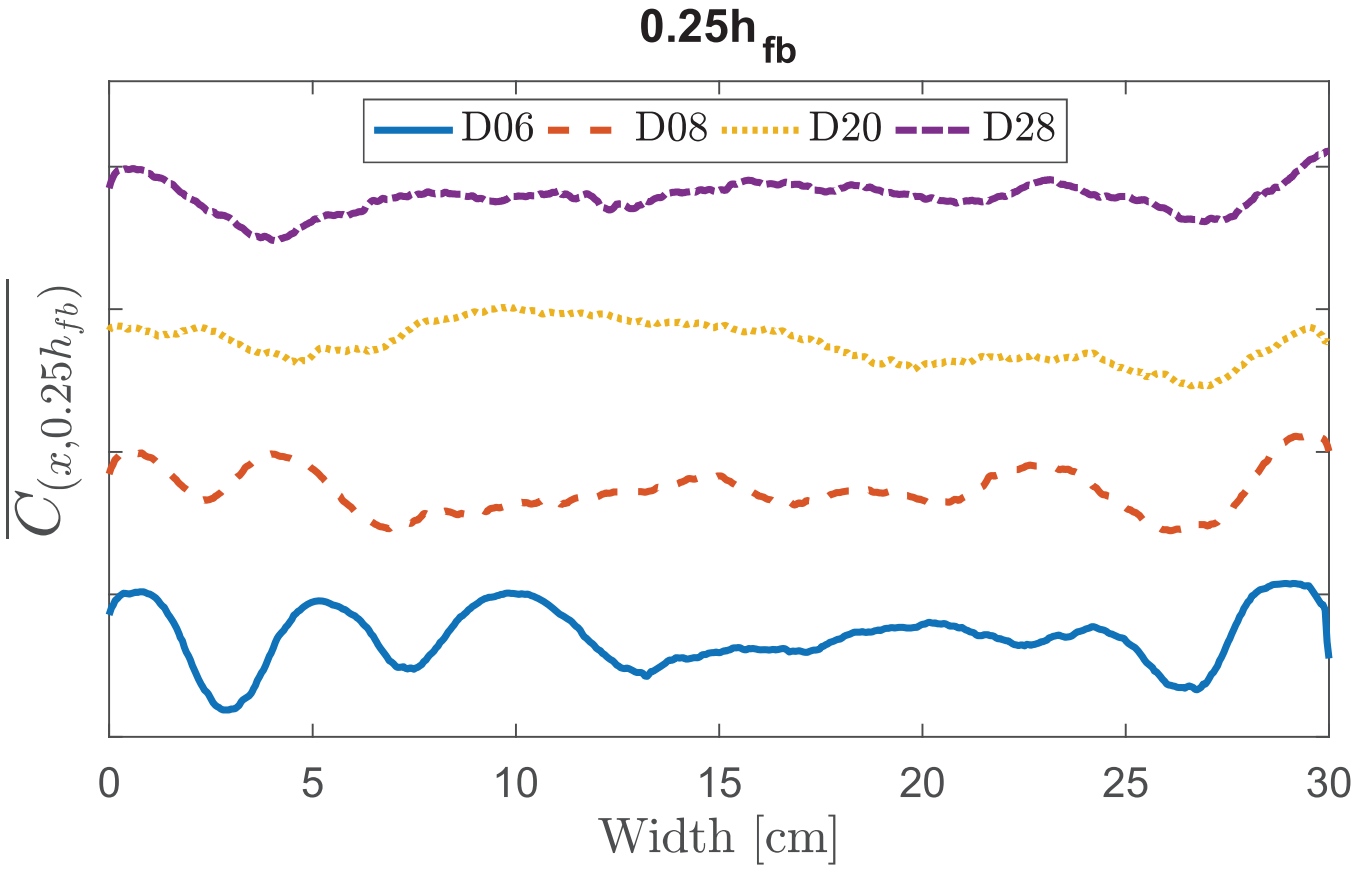

Figure
Click here to download Figure: Figure3_1_b.eps

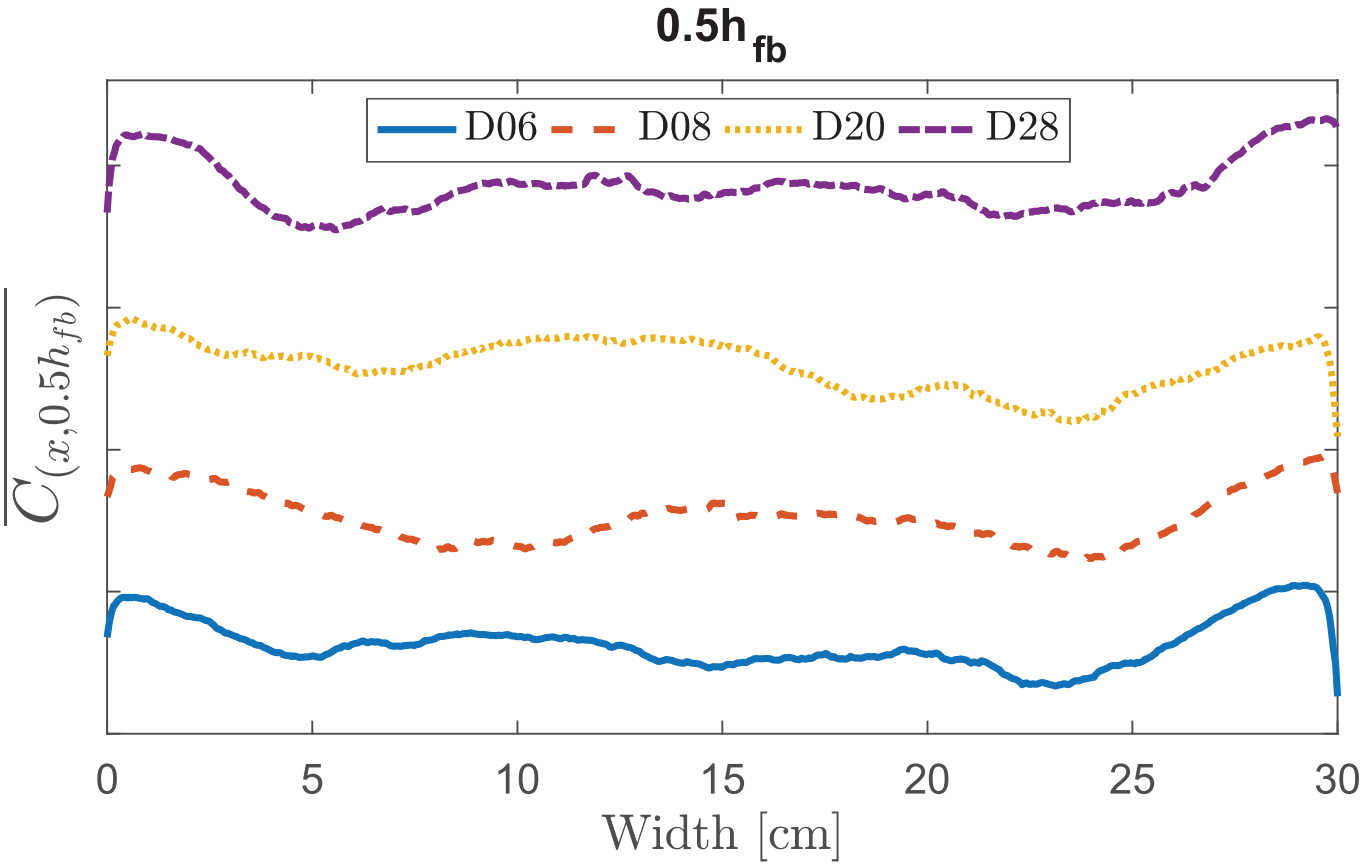

Figure
Click here to download Figure: Figure3_1_c.eps

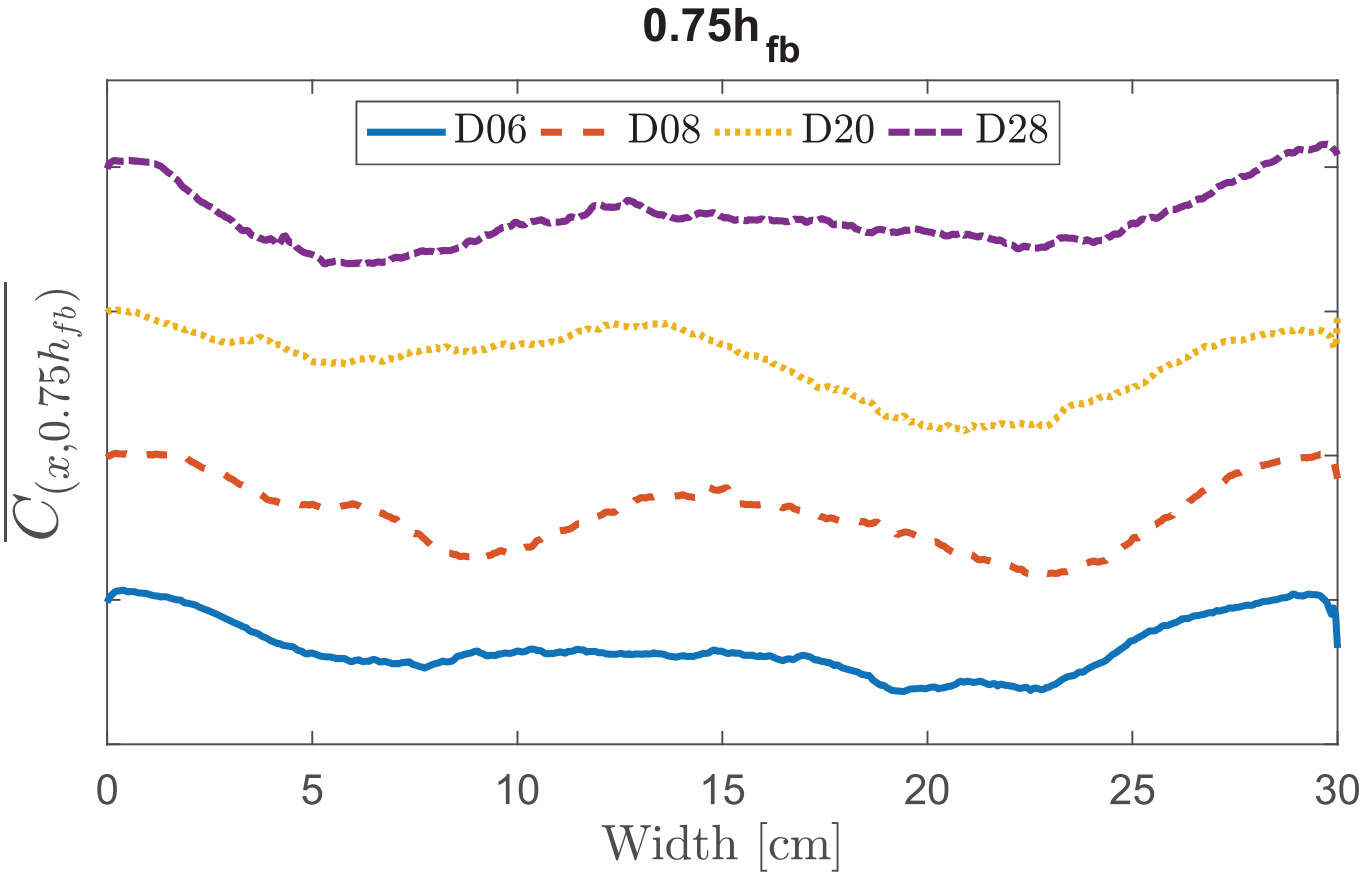

Figure
Click here to download Figure: Figure3_2_a.eps

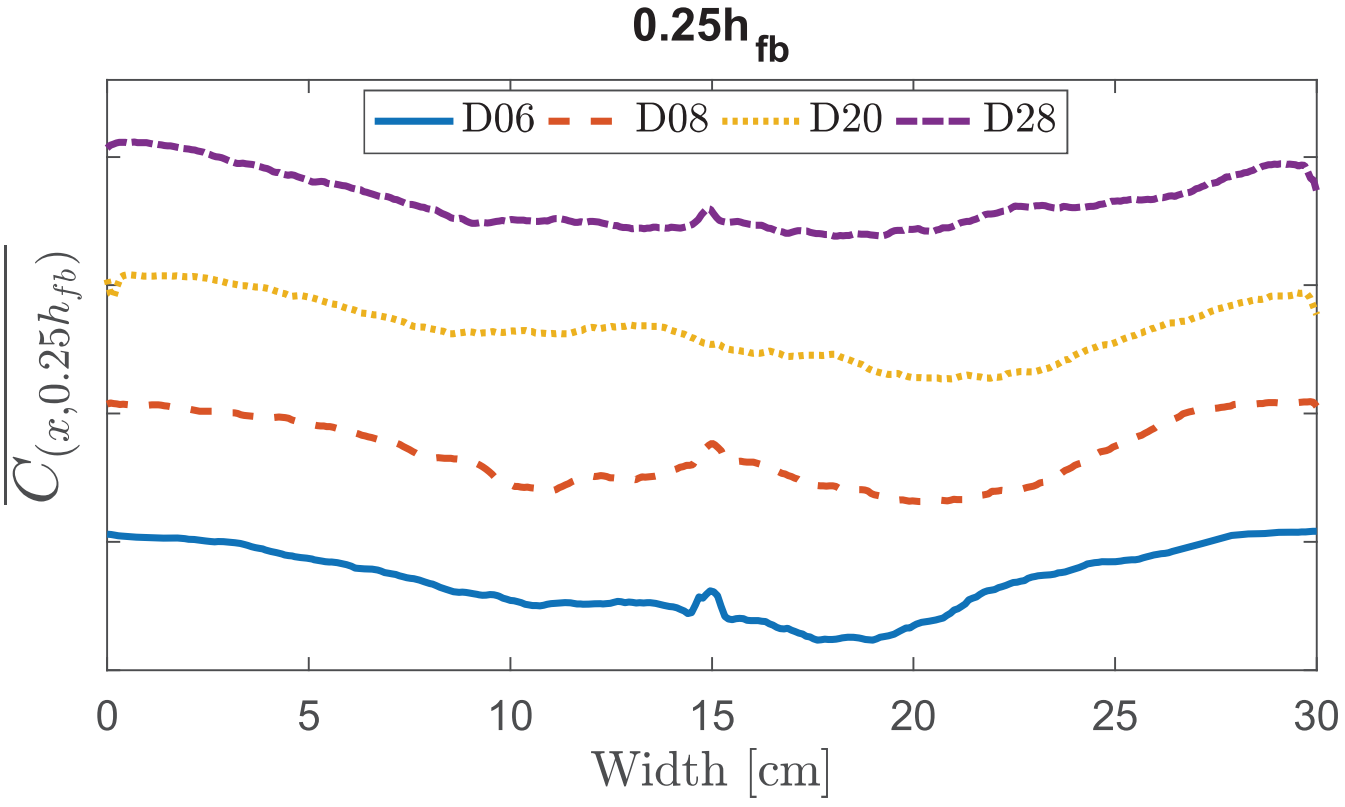

Figure
Click here to download Figure: Figure3_2_b.eps

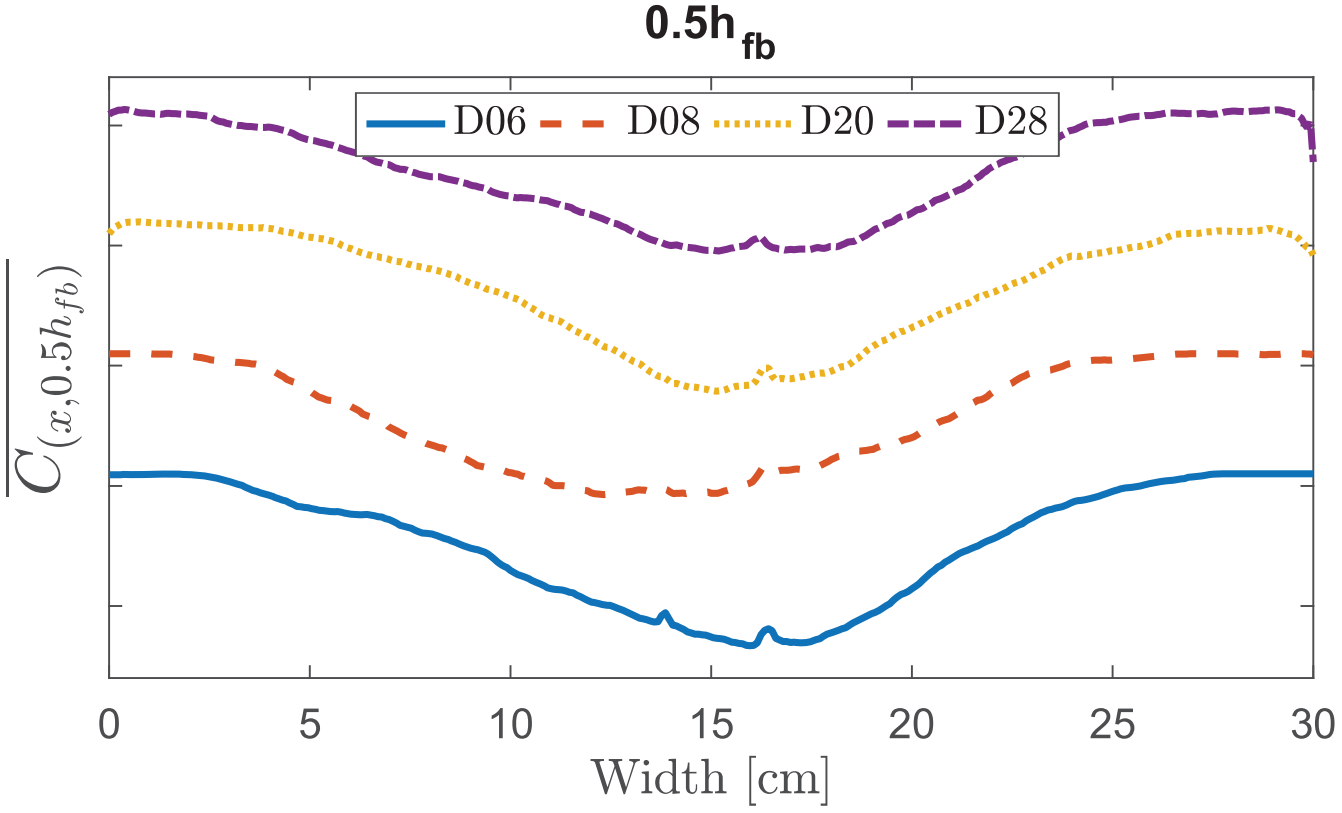

Figure
Click here to download Figure: Figure3_2_c.eps

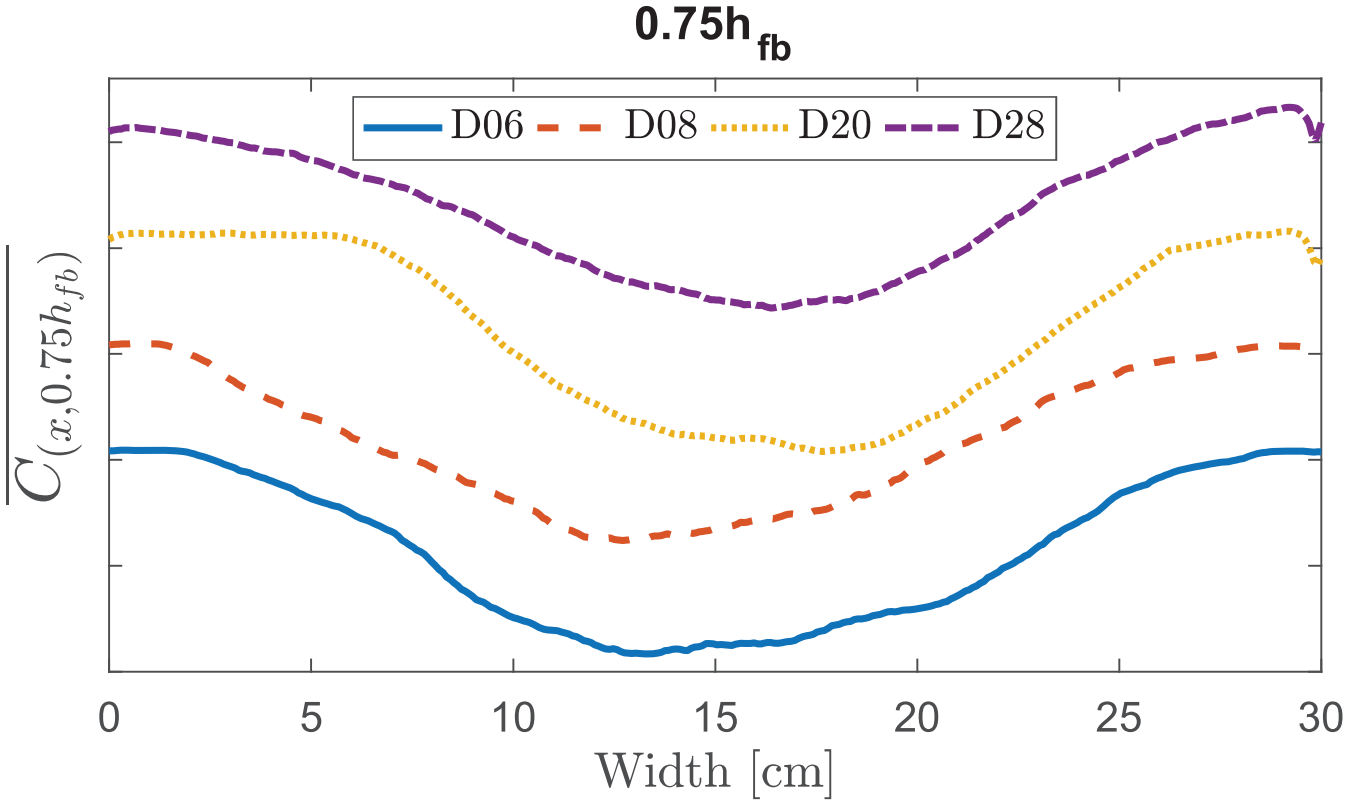

Figure
Click here to download Figure: Figure4_1.eps

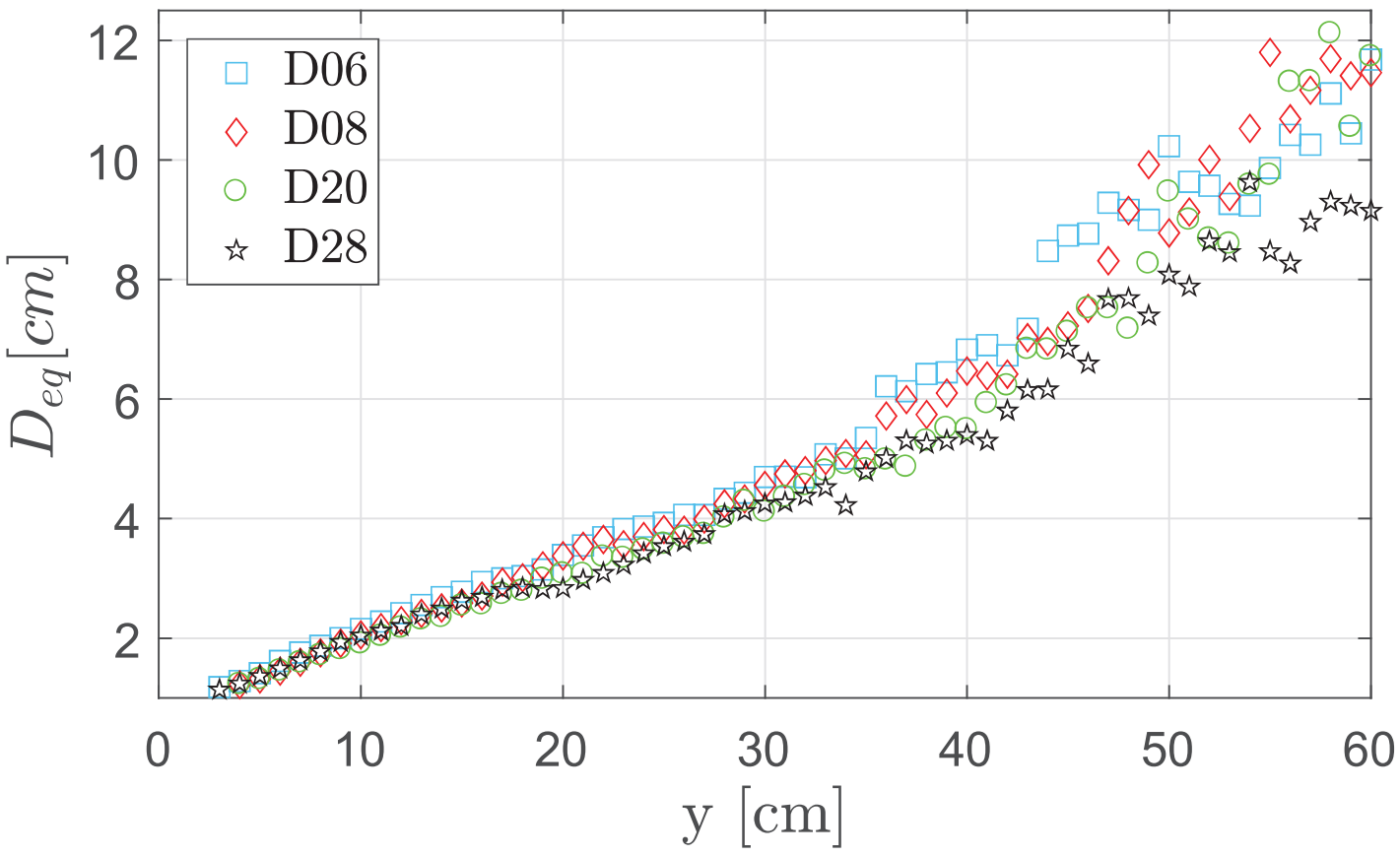

Figure
Click here to download Figure: Figure4_2.eps

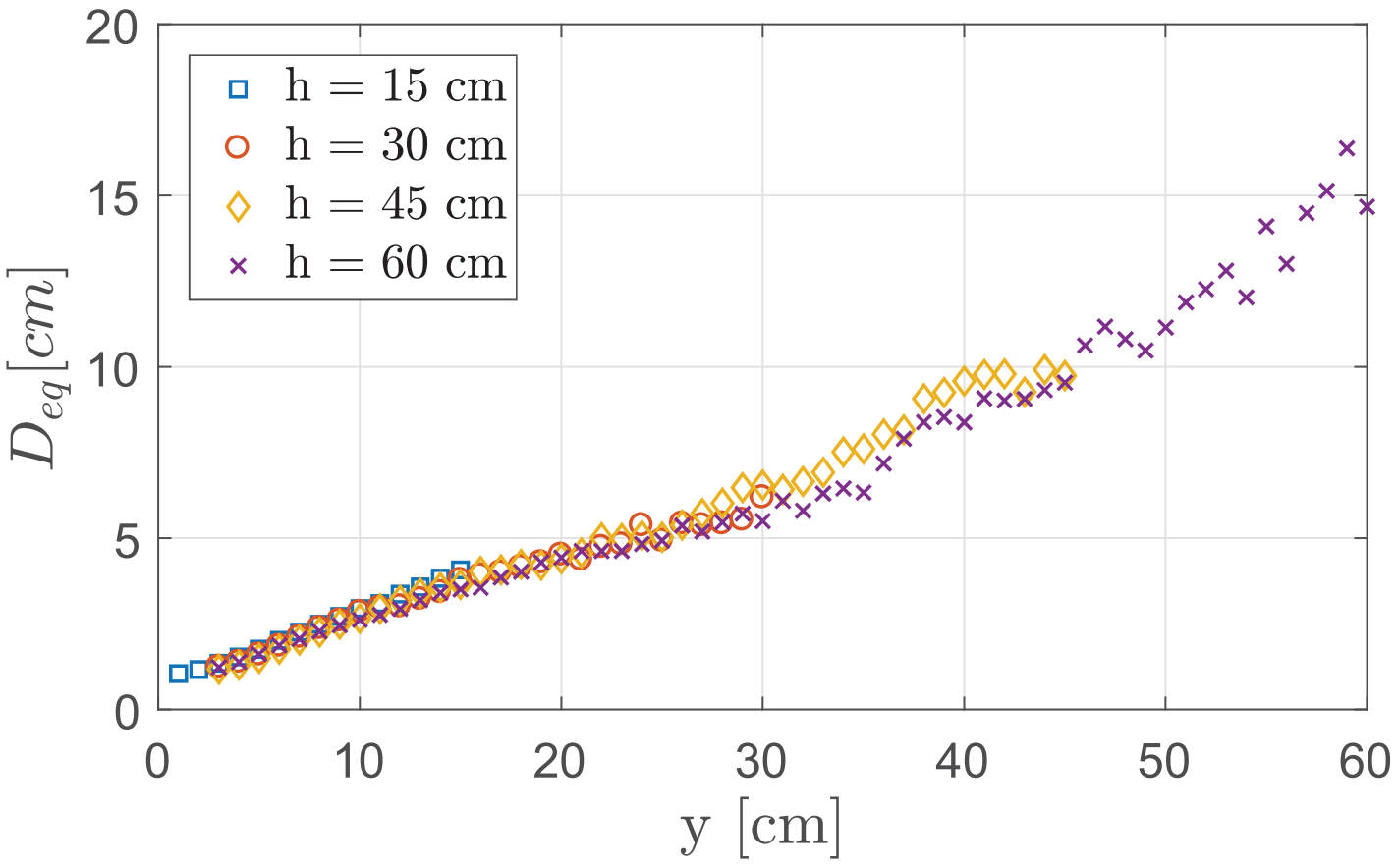

Figure
Click here to download Figure: Figure5.eps

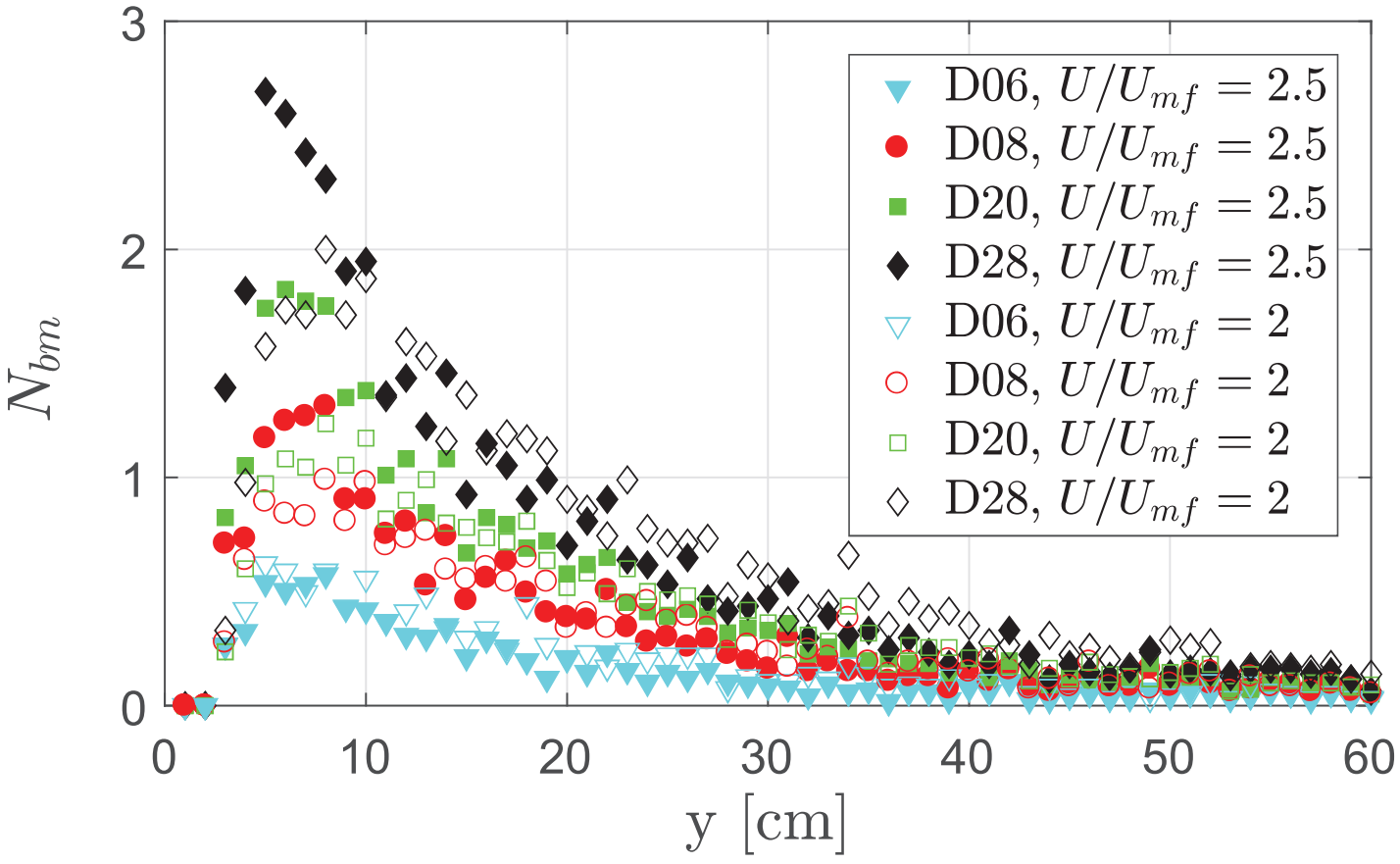

Figure
Click here to download Figure: Figure6.eps

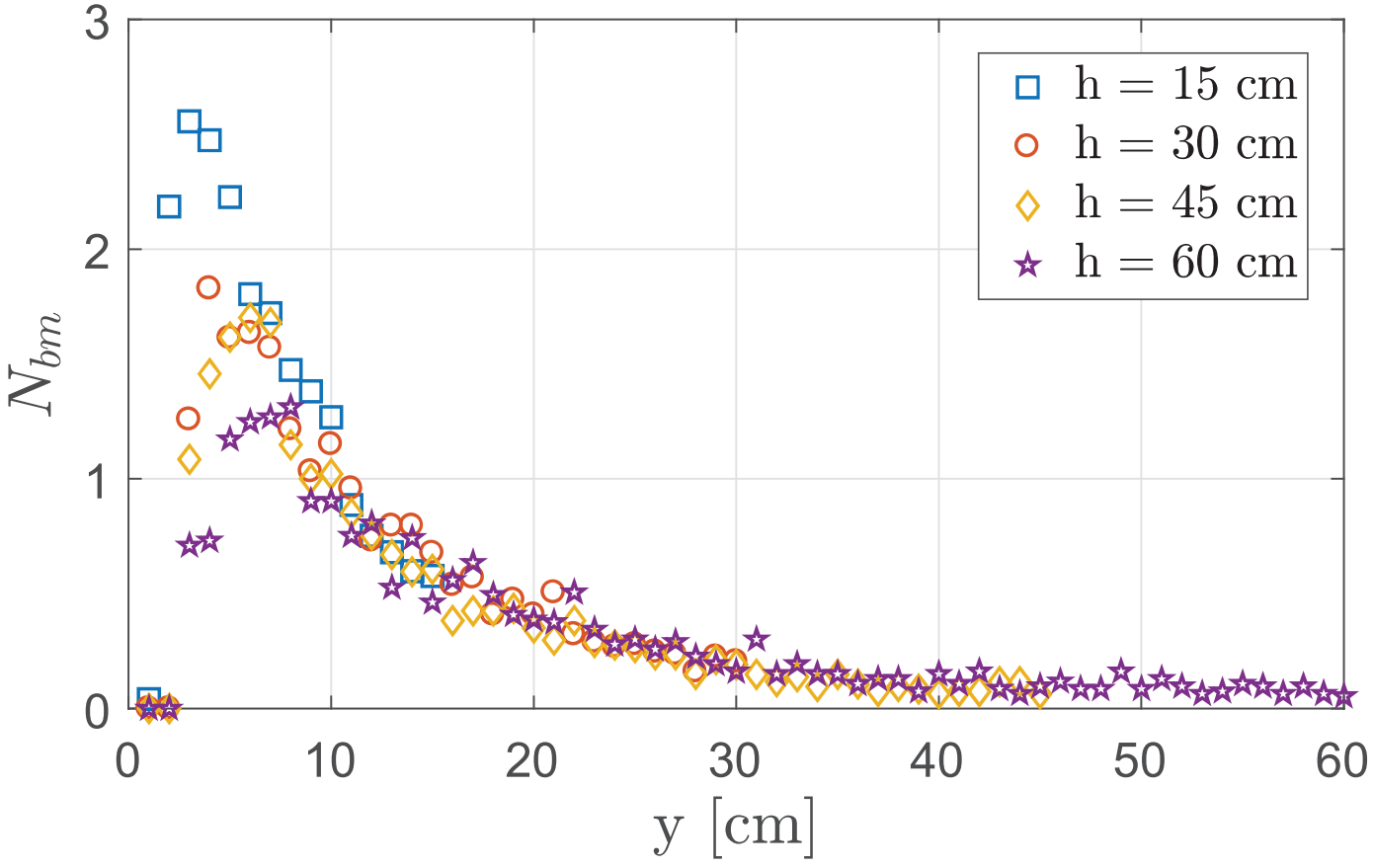

Figure

Click here to download Figure: Figure7_1_a.eps

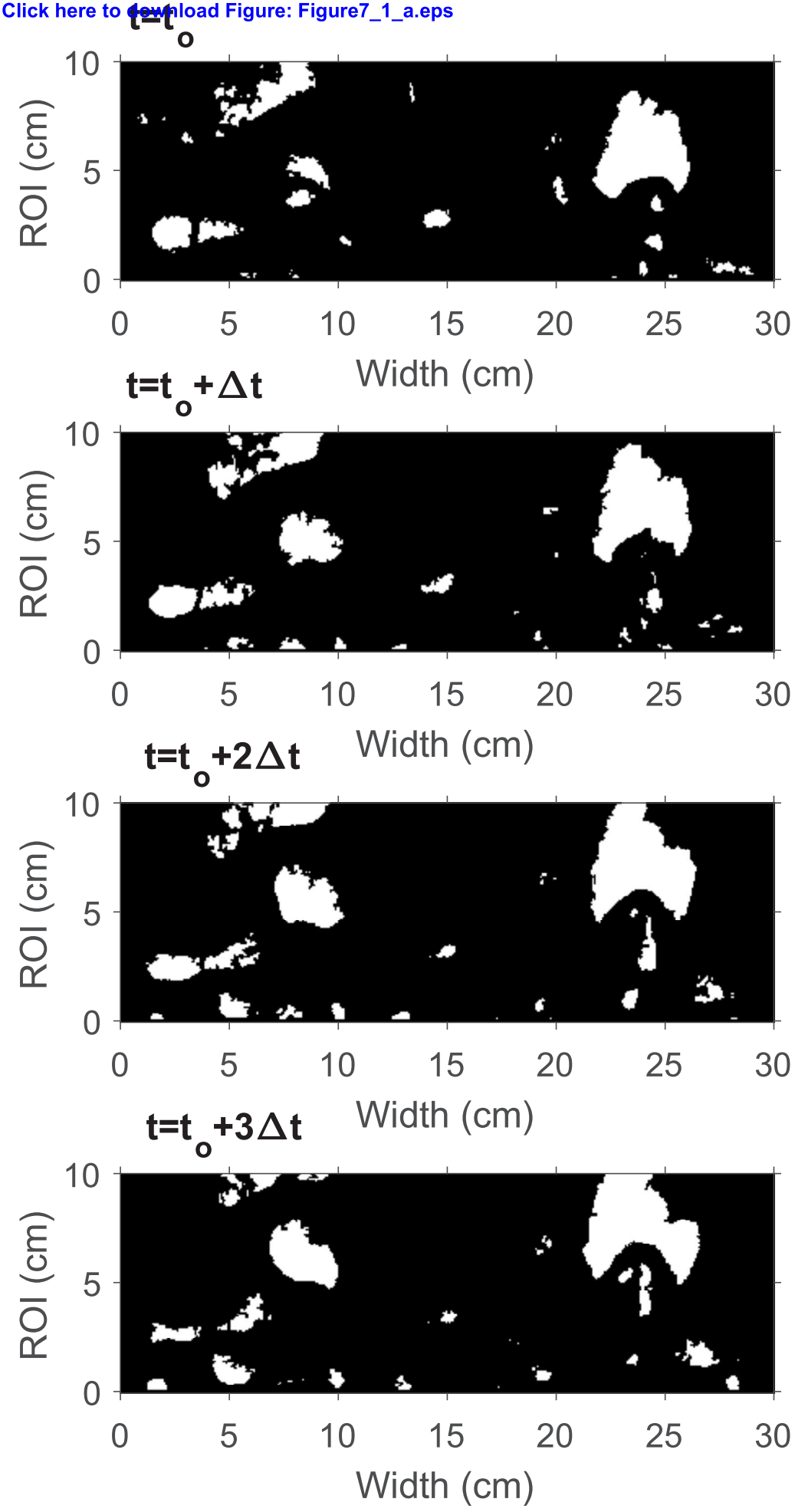

Figure
Click here to download Figure: Figure7_1_b.eps

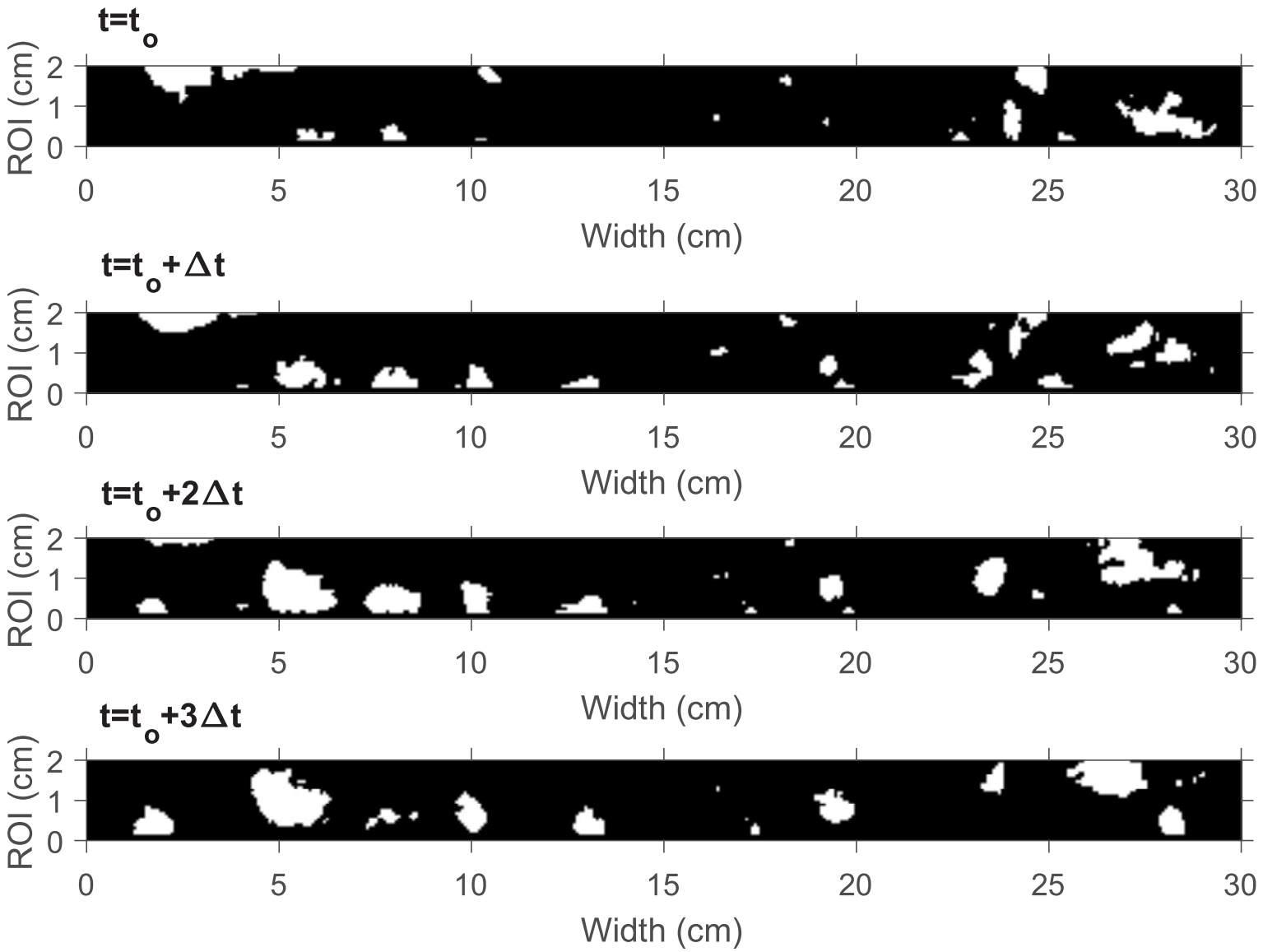

Figure
Click here to download Figure: Figure7_2_a.eps

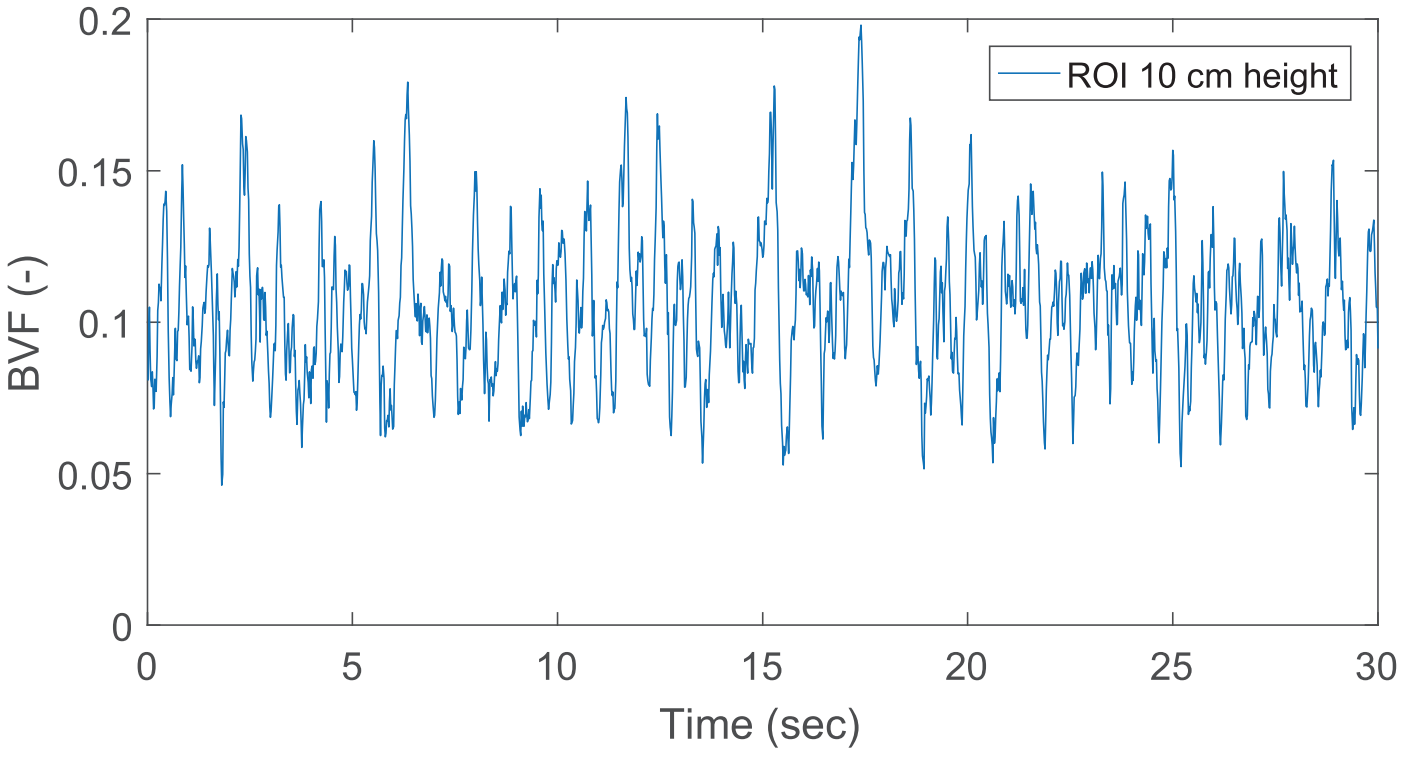

Figure
Click here to download Figure: Figure7_2_b.eps

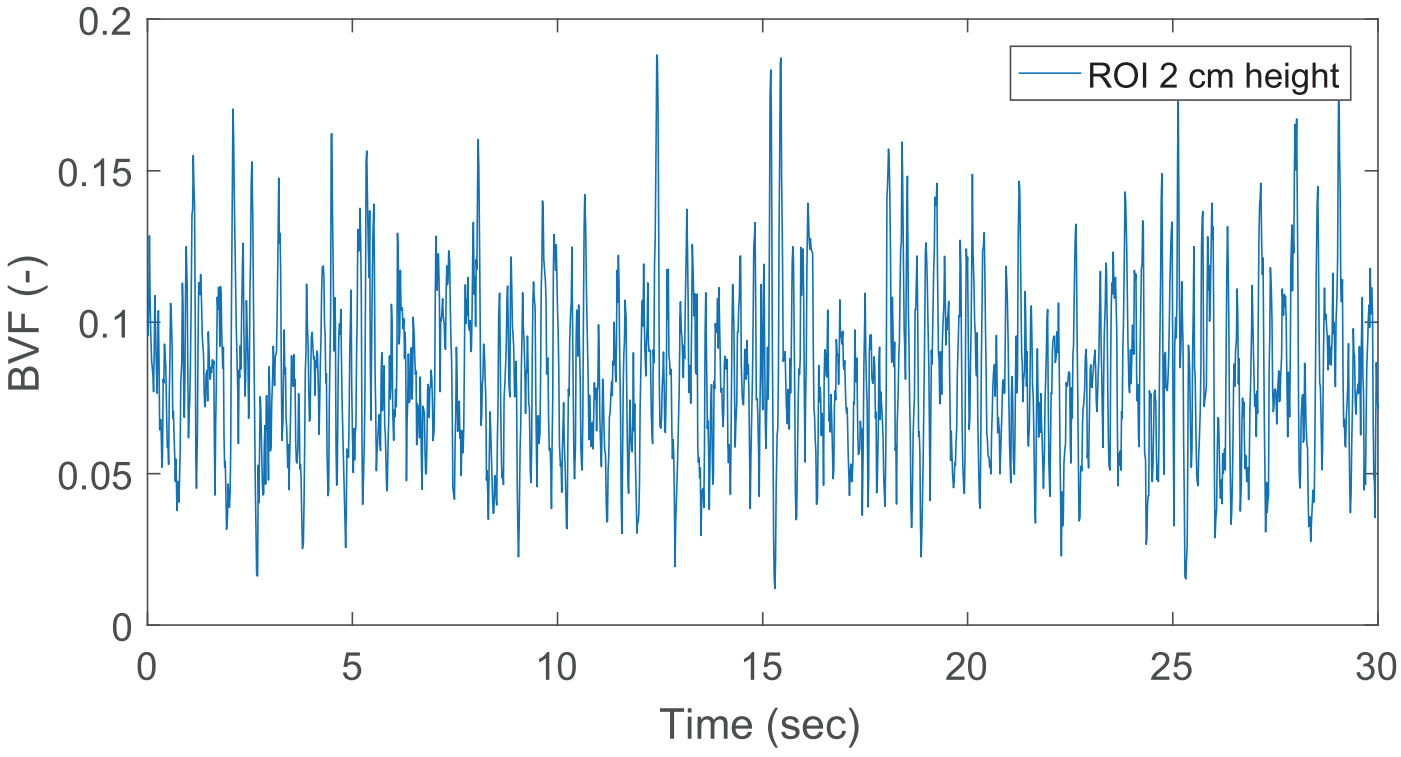

Figure
Click here to download Figure: Figure8_a.eps

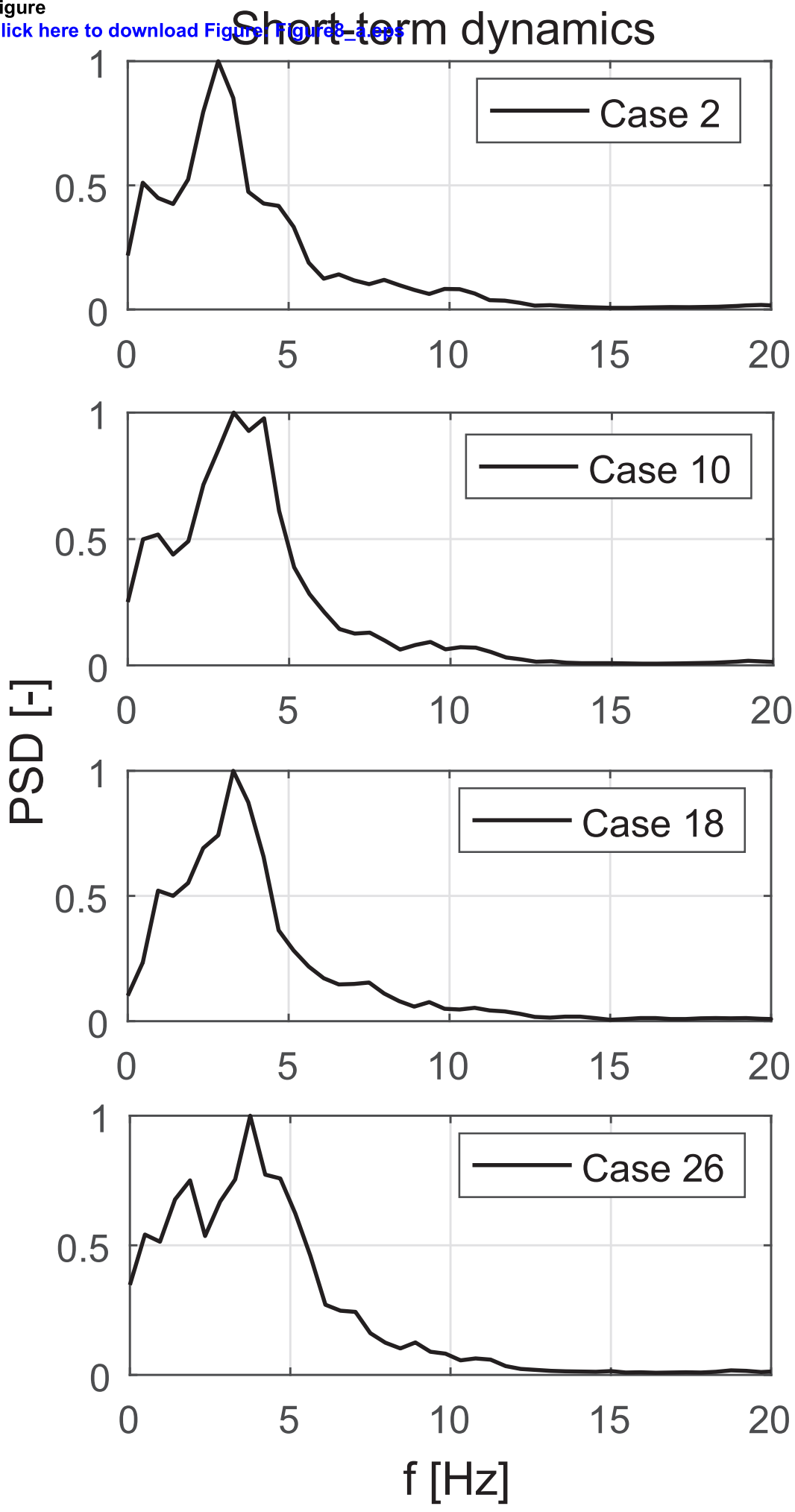

Figure
Click here to download Figure: Figure8_b.eps

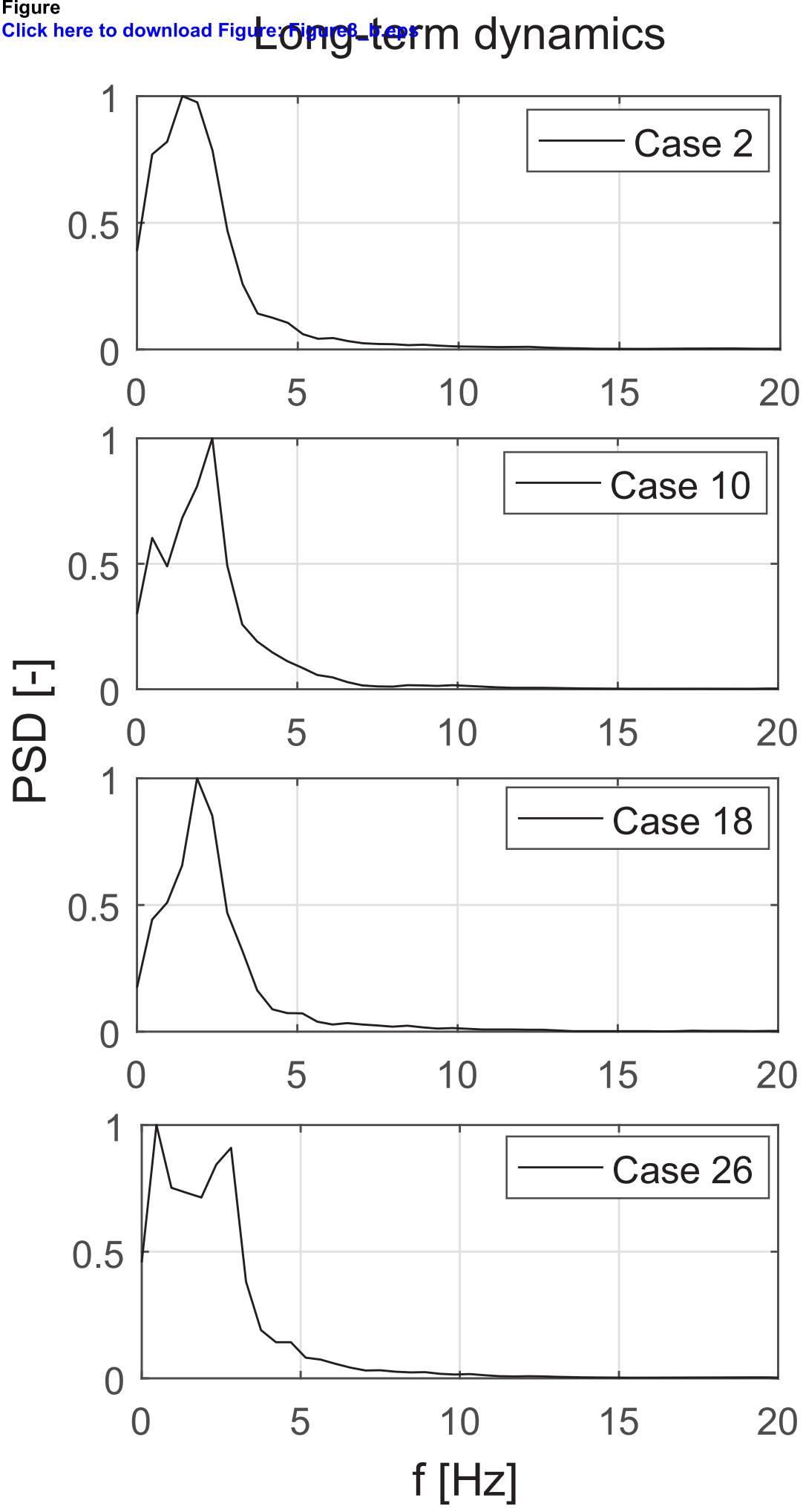

Figure
Click here to download Figure: Figure9.eps

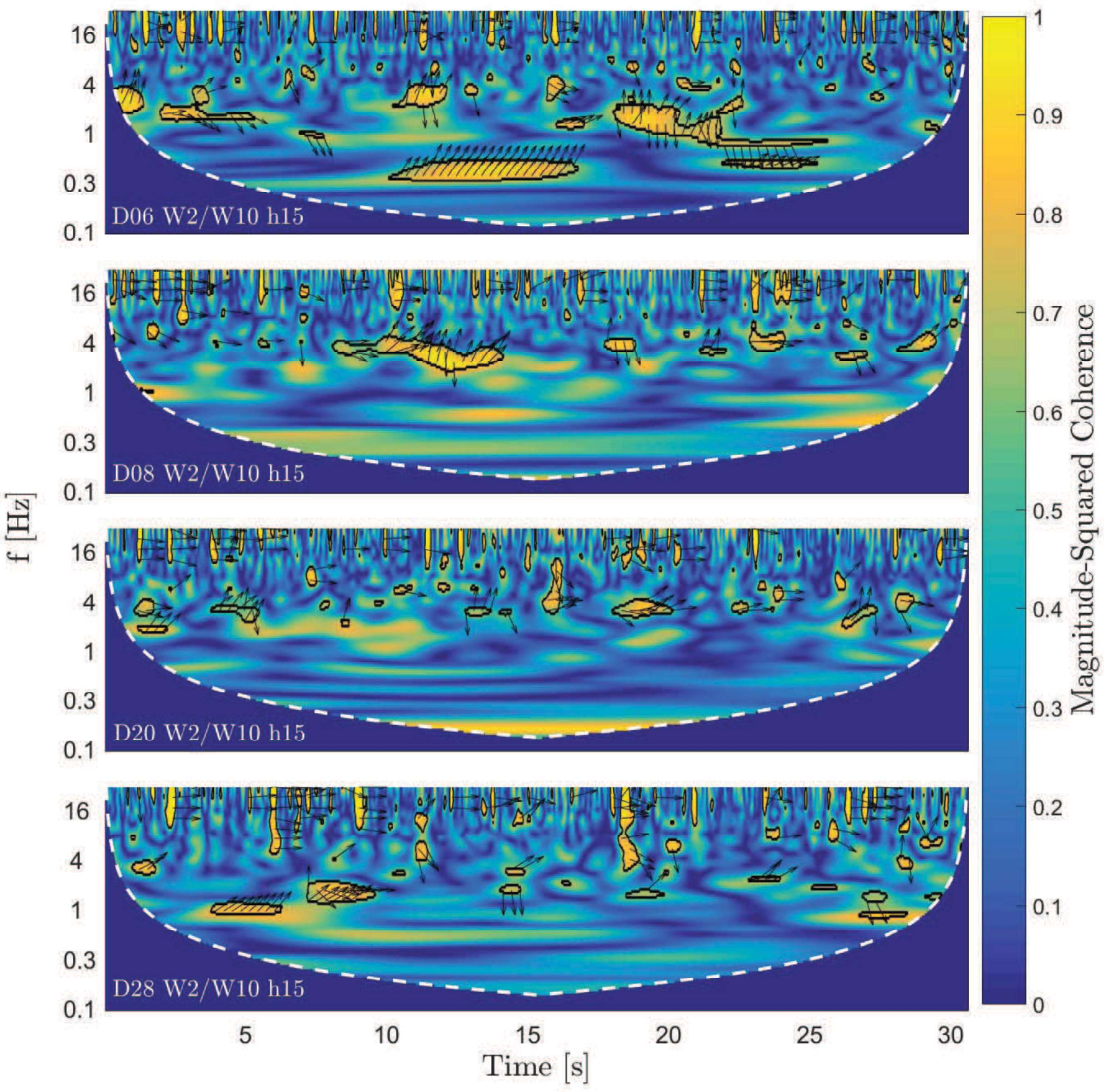

Figure
Click here to download Figure: Figure10_a.eps

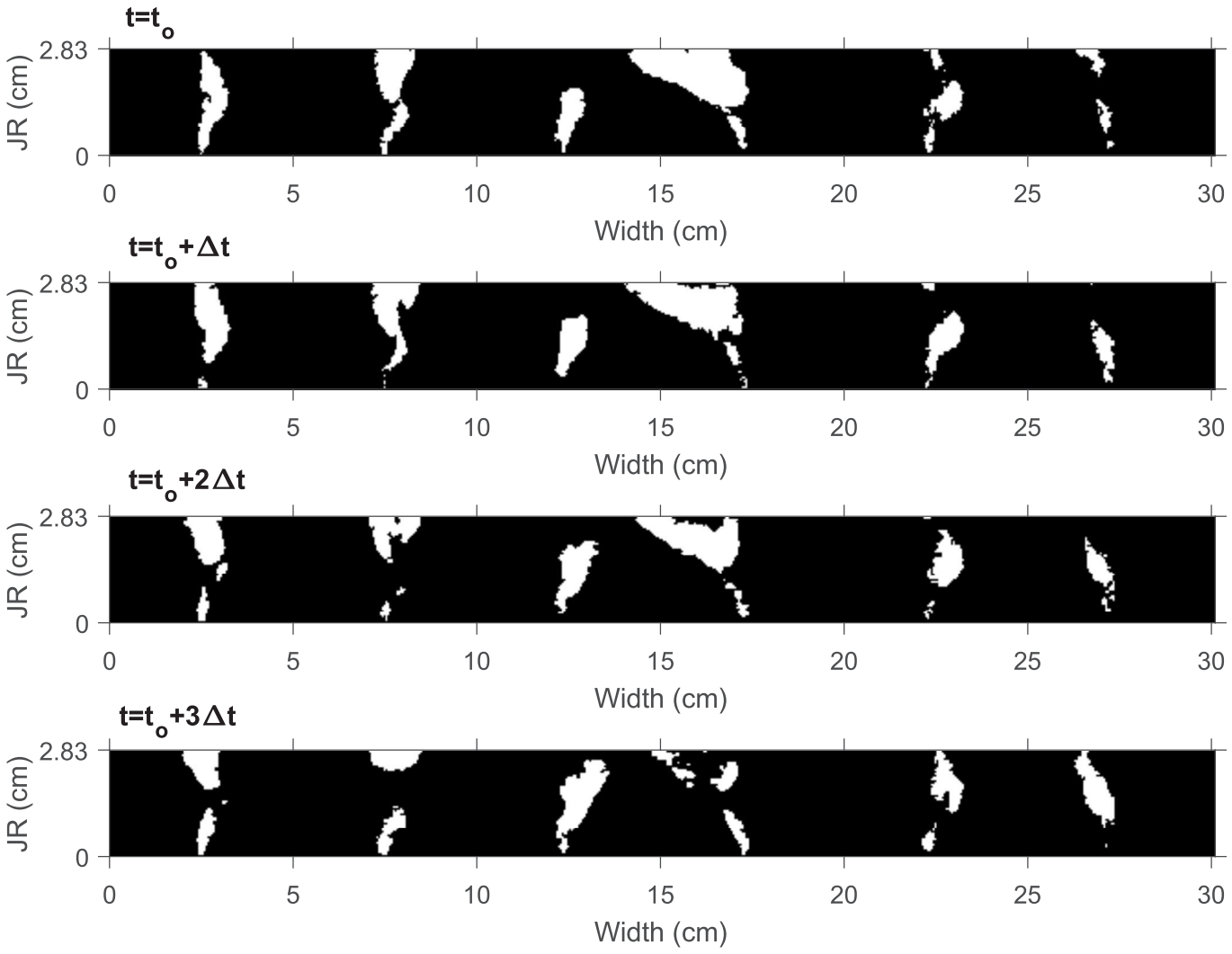

Figure
Click here to download Figure: Figure10_b.eps

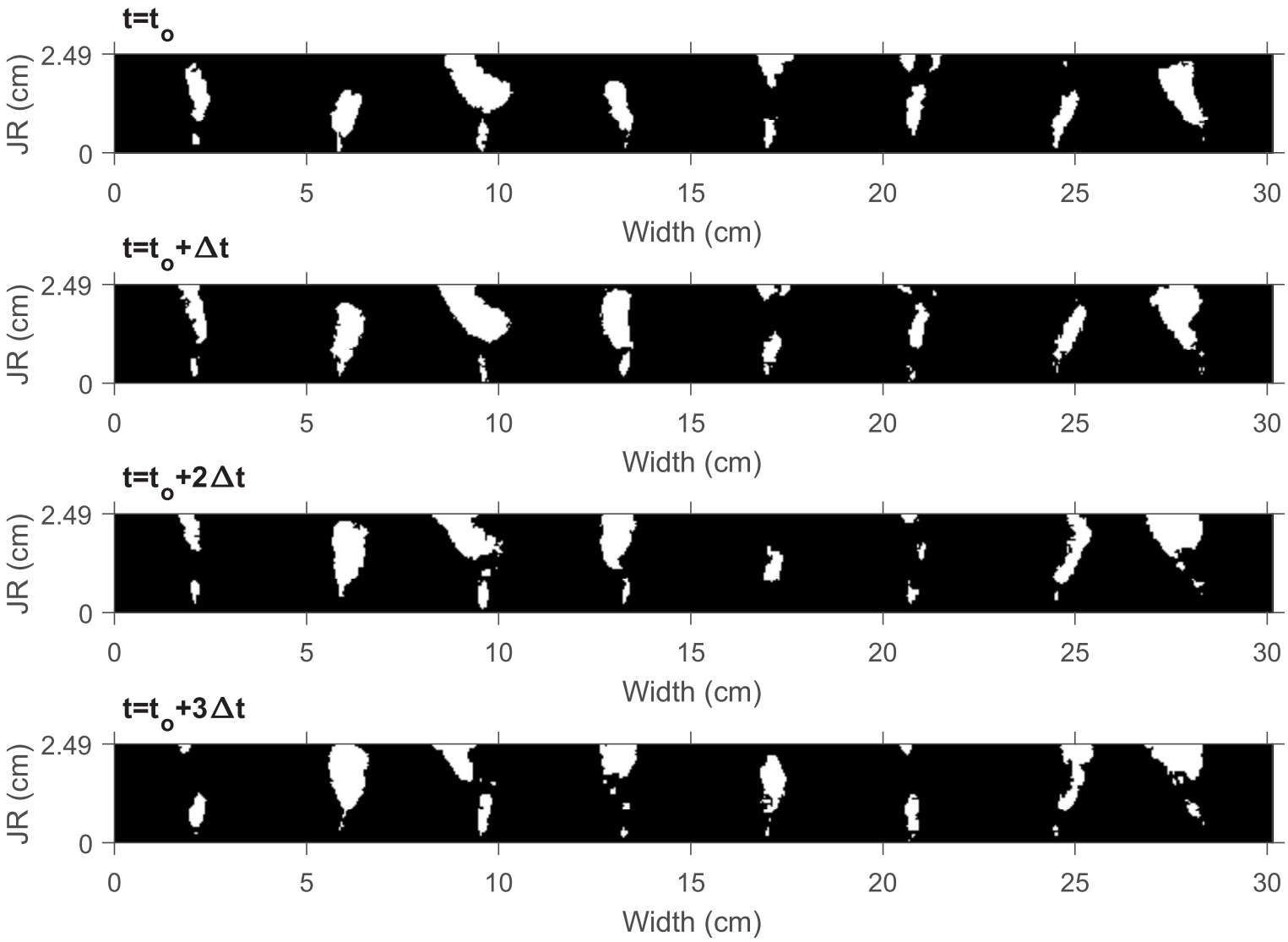

Figure
Click here to download Figure: Figure10_c.eps

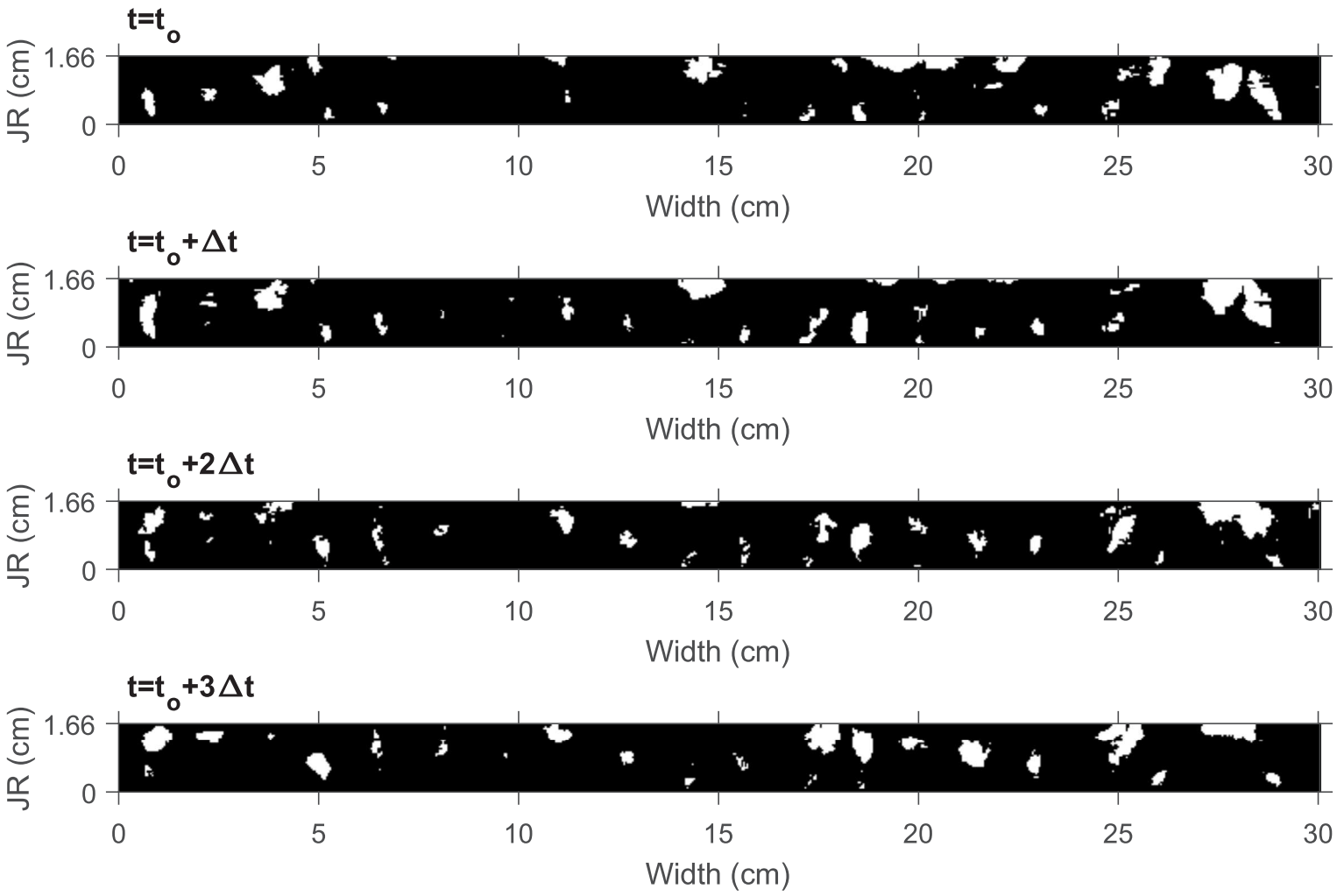

Figure
Click here to download Figure: Figure11_1.eps

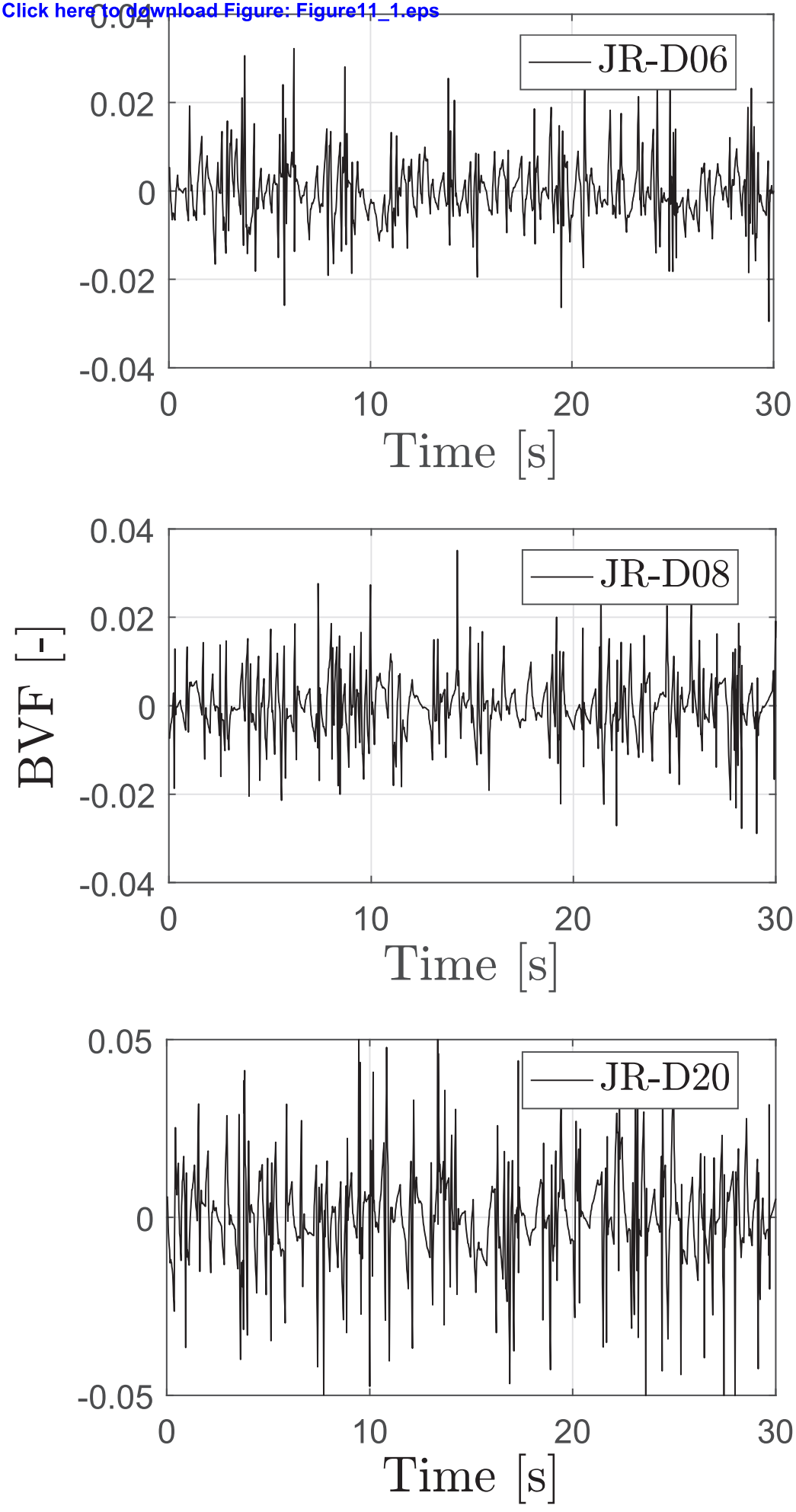

Figure
Click here to download Figure: Figure11_2.eps

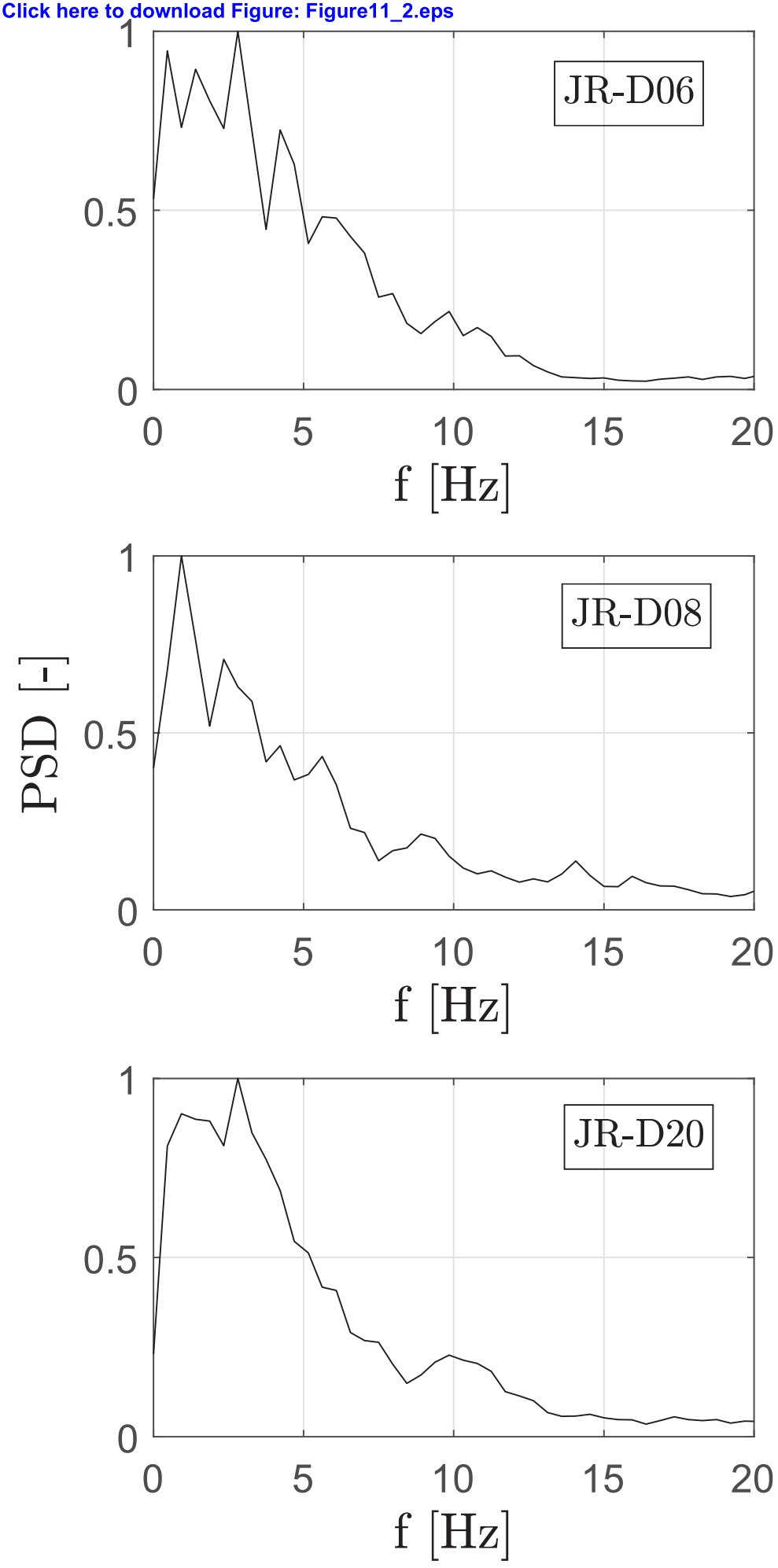

Figure
Click here to download Figure: Figure12.eps

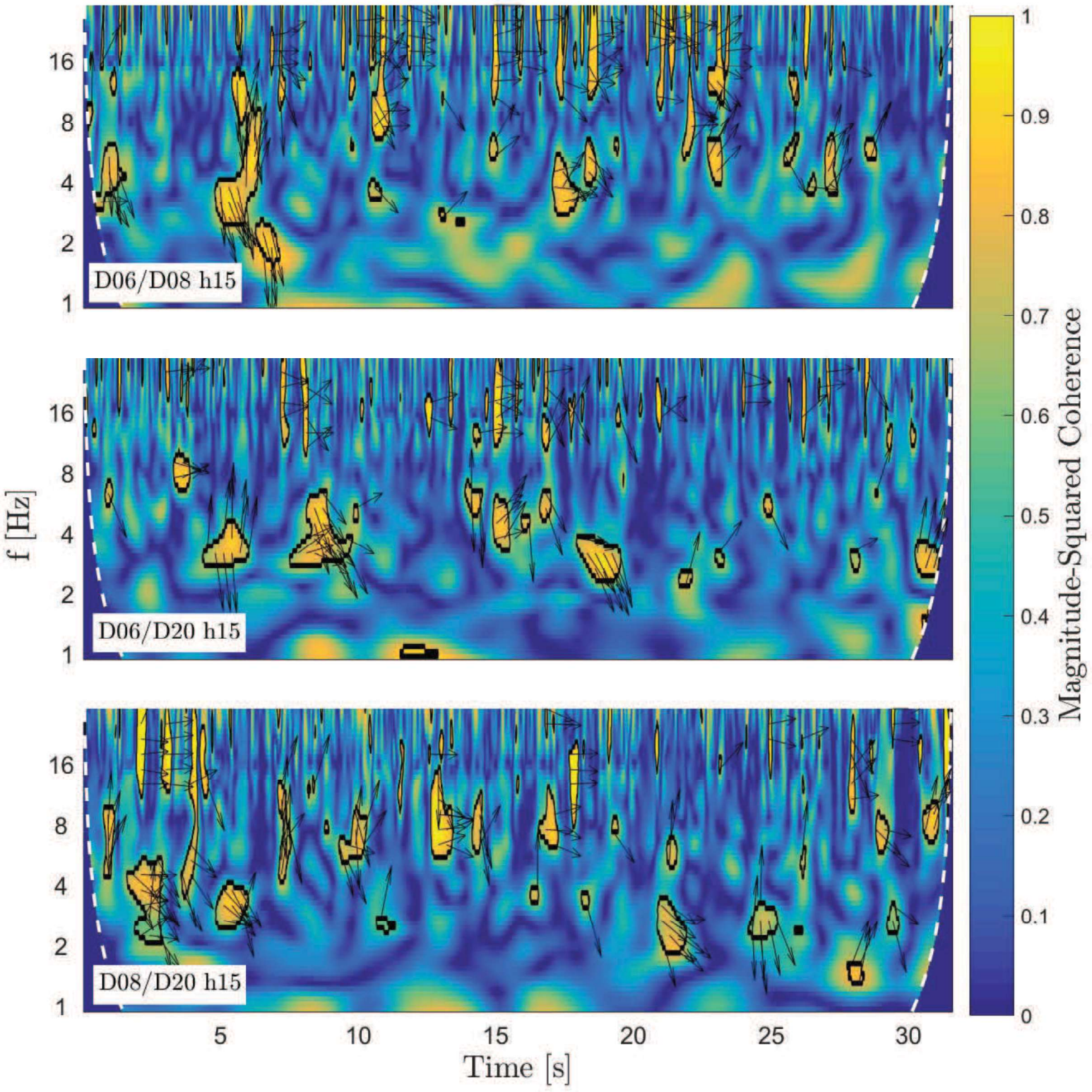

Figure
Click here to download Figure: Figure13.eps

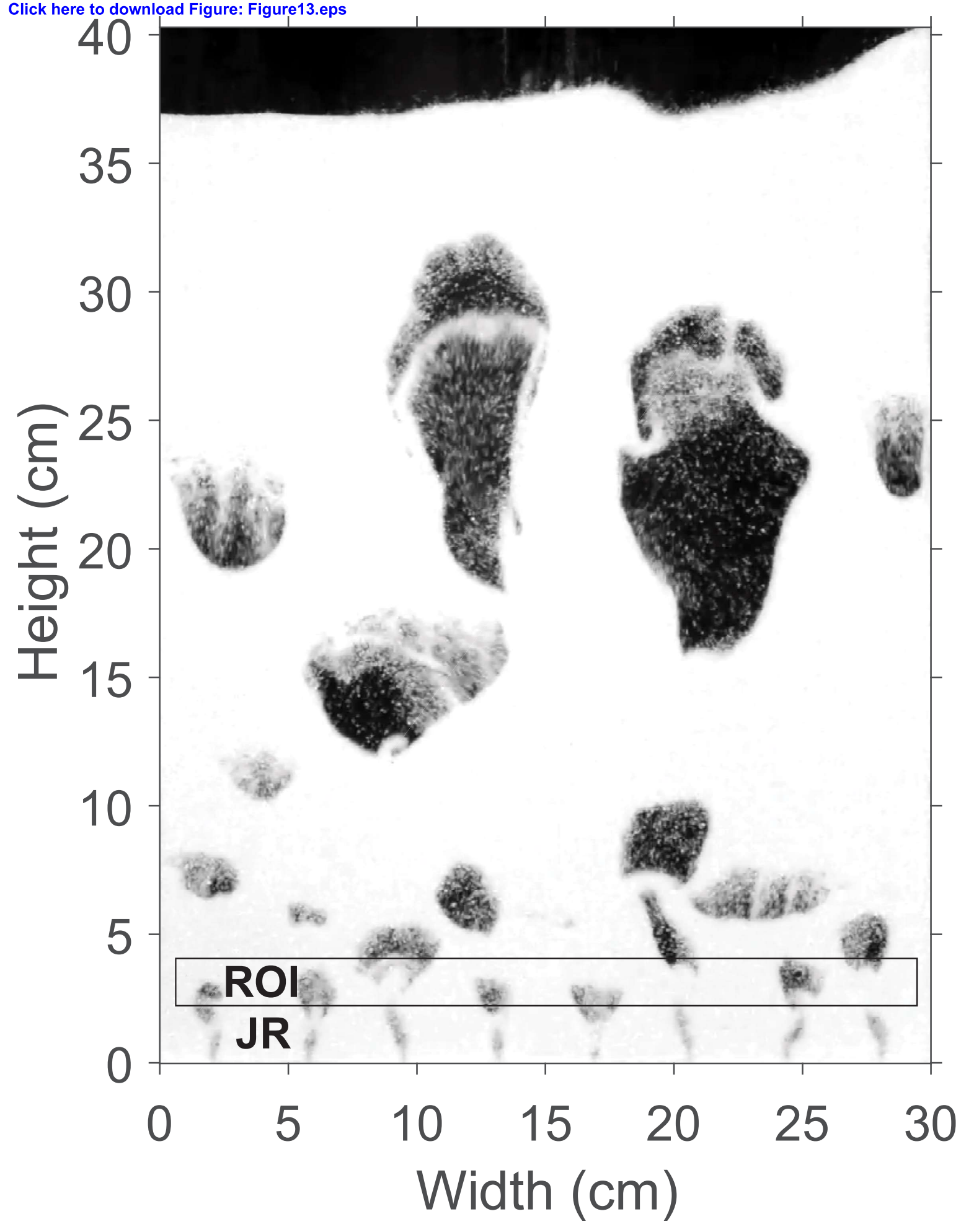

Figure
Click here to download Figure: Figure14_1.eps

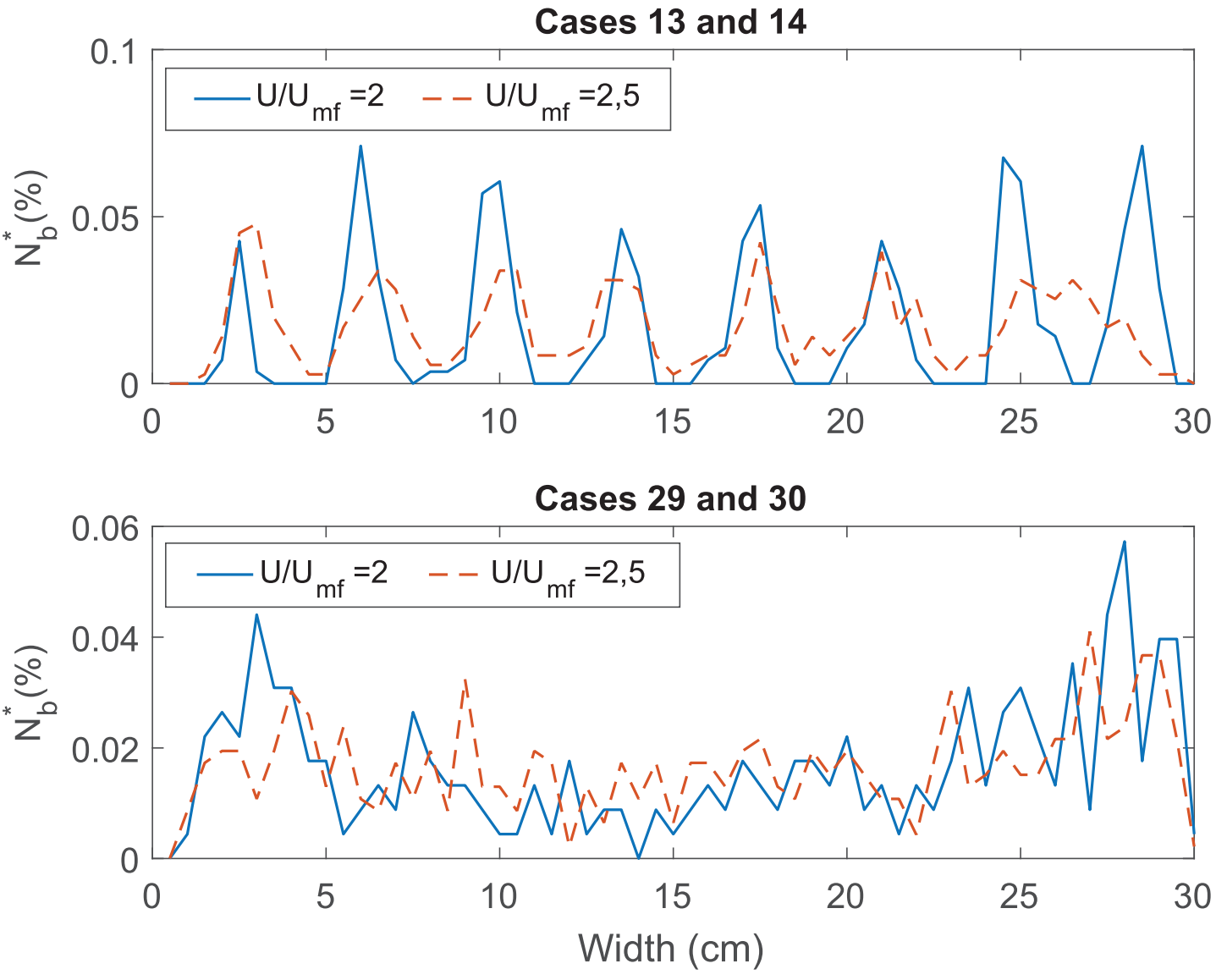

Figure
Click here to download Figure: Figure14_2.eps